Solvent Polarity Predictably Tunes Spin Crossover $T_{1/2}$ in Isomeric Iron(II) Pyrimidine Triazoles

Santiago Rodríguez-Jiménez, Alexis S. Barltrop, Nicholas G. White,
Humphrey L. C. Feltham, and Sally Brooker*

Department of Chemistry and MacDiarmid Institute for Advanced Materials and Nanotechnology, University of Otago, PO Box 56, Dunedin, 9054, New Zealand

Contents

S1. NMR spectroscopy

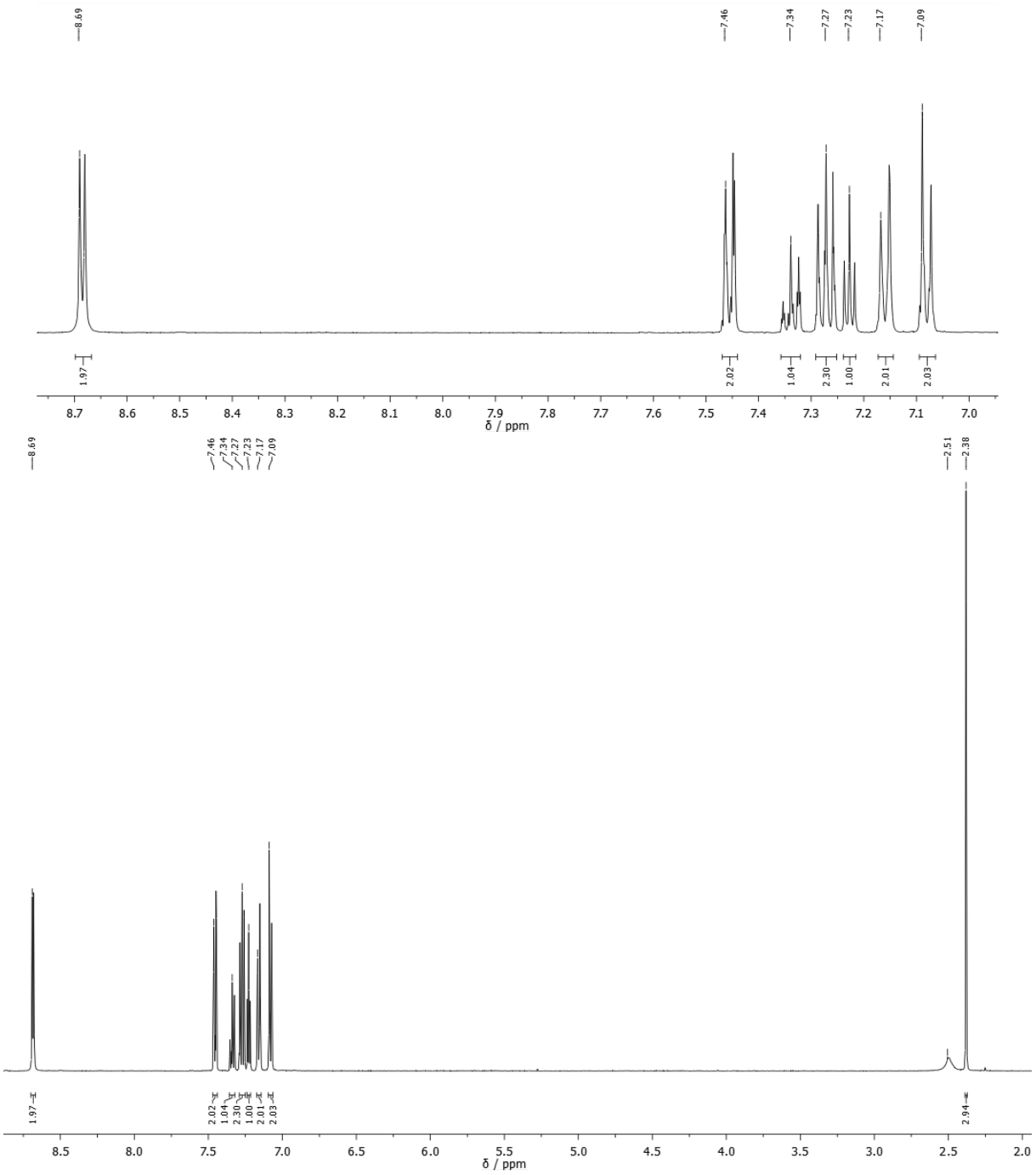

Figure S1. ^{1}H NMR spectra of ligand **L^{2pyrimidine}** at 500 MHz in $CDCl_3$ at 25°C. (Top) expansion of aromatic region from 9 to 7 ppm, (bottom) full-range spectrum.

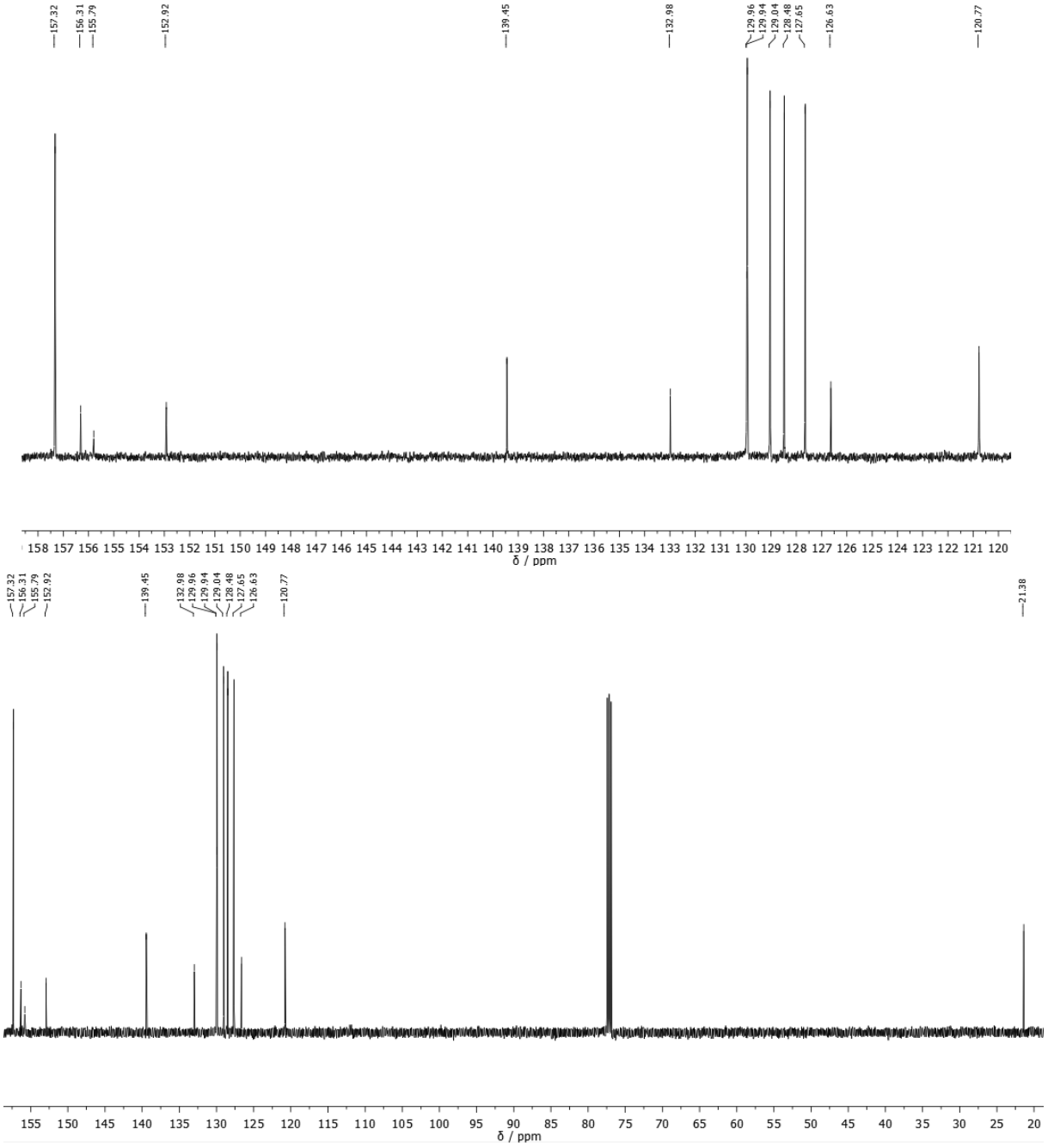

Figure S2. ^{13}C NMR spectra of ligand **L^{2pyrimidine}** at 125 MHz in $CDCl_3$ at 25°C. (Top) expansion spectrum from 158 to 120 ppm, (bottom) full-range spectrum.

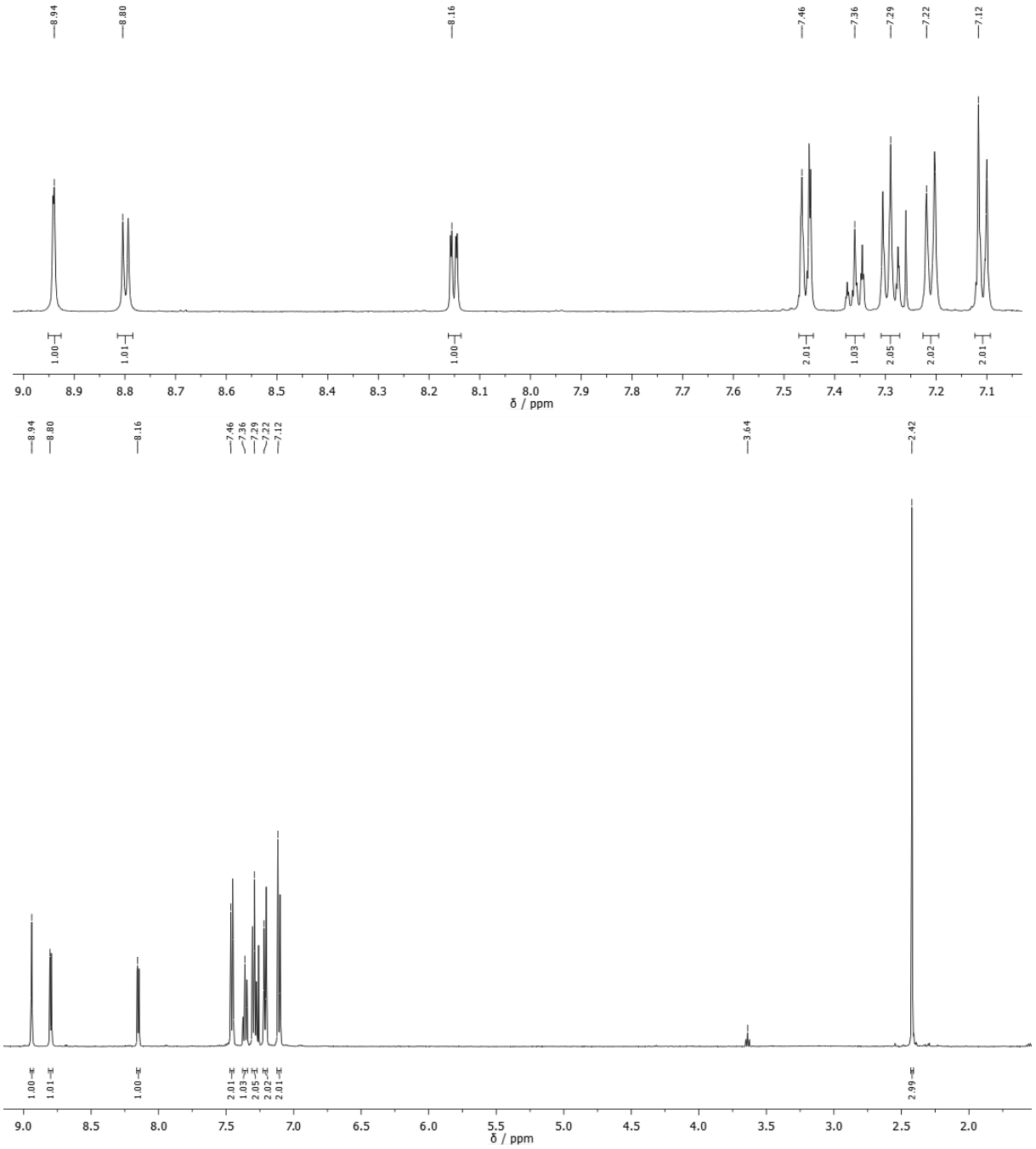

Figure S3. ^{1}H NMR spectra of ligand **L^{4pyrimidine}** at 500 MHz in $CDCl_3$ at 25°C. (Top) expansion of aromatic region from 9 to 7 ppm, (bottom) full-range spectrum.

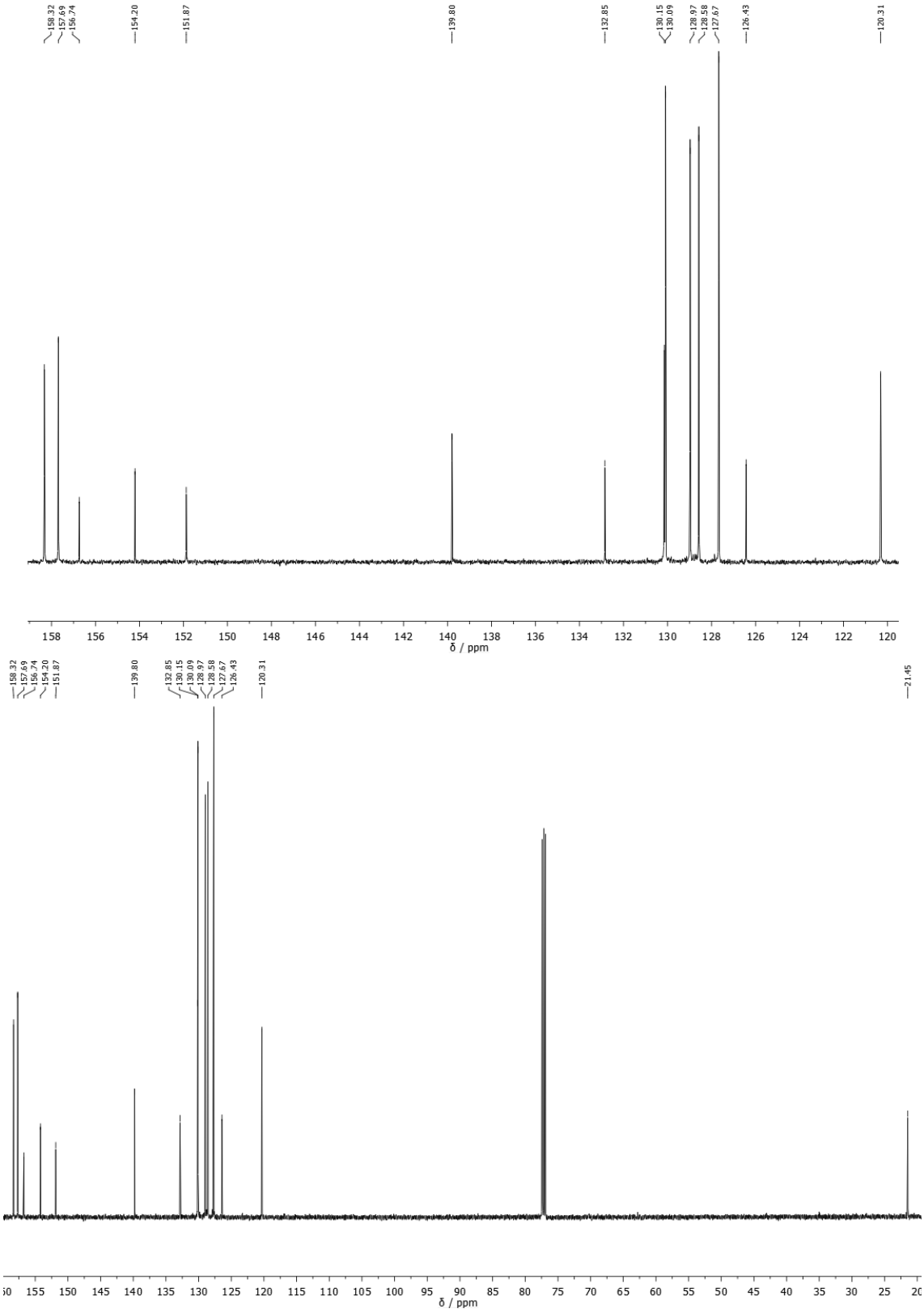

Figure S4. ^{13}C NMR spectra of ligand $\mathbf{L^{4pyrimidine}}$ at 125 MHz in $CDCl_3$ at 25°C. (Top) expansion spectrum from 158 to 120 ppm, (bottom) full-range spectrum.

S2. Single crystal structure analysis

S2.1. Refinement details

Single-crystal X-ray diffraction measurements were collected on an Oxford Diffraction SuperNova diffractometer with Atlas CCD, equipped with a Cryostream N2 open-flow cooling device, [1] using mirror monochromated micro-focus Mo or Cu-Kα radiation at 100 K. Series of scans were performed in such a way as to collect a complete set of unique reflections to a maximum resolution of 0.80 Å. Raw frame data (including data reduction, inter-frame scaling, unit cell refinement and absorption corrections)[2] for all structures were processed using CrysAlis Pro.[3] Structures were solved using SUPERFLIP[4] and refined using full-matrix least-squares on F^2 and refined against F^2 using all data by full-matrix least-squares techniques with SHELXS-2014[5] and refined using full-matrix least-squares on F^2 within the X-Seed graphical user interface. All hydrogen atoms were inserted at calculated positions with U(H) = 1.2 U(attached atom), and rode on the atoms to which they were attached, unless otherwise stated. Crystallographic data for the structures have been deposited with the Cambridge Crystallographic Data Centre, CCDC 1547039-1547044 and 1816482.

L^{4pyrimidine}. (Figure S6) Whole ligand is in the asymmetric unit (the other three ligand molecules in the unit cell are generated through a glade plane, an inversion and a 2-fold rotation (Z=4)). No solvent of crystallization. All non-H atoms refined anisotropically. Residual e$^-$ density +0.397/-0.275 eÅ^3. Q peaks were used as a guide to insert hydrogen atoms at the calculated positions. This enabled clear identification of the phenyl and pyrimidine rings as these could be distinguished by the number of visible Q peaks (hydrogen atoms), with five for the phenyl ring and only three for the pyrimidine ring. To certify that the assigned carbon and nitrogen atoms had U_{eq} values within an accepted range the type of atoms, i.e. C or N, was changed and compared with the location of the Q peaks/hydrogens showing concurring results. This enabled clear identification of the phenyl and pyridine rings.

[Fe^{II}(**L^{2pyrimidine}**)$_2$(NCS)$_2$] (**1**). (Figures 1 and S7) Half of this complex is in the asymmetric unit (other half generated by inversion). No solvent of crystallization. No disorder. All non-H atoms refined anisotropically. Residual e$^-$ density +0.301/-0.327 eÅ^3.

[Fe^{II}(**L^{2pyrimidine}**)$_2$(NCSe)$_2$] (**2**). (Figure S8) Half of this complex is in the asymmetric unit (other half generated by inversion). No solvent of crystallization. No disorder. All non-H atoms refined anisotropically. Residual e$^-$ density +0.467/-0.418 eÅ^{-3}.

[Fe^{II}(**L^{2pyrimidine}**)$_2$(NCBH3)$_2$]·2CHCl$_3$ (**3**·2CHCl$_3$). (Figures 3 and S11) Half of the complex present in the asymmetric unit and the other half generated by inversion. All non-H atoms are refined anisotropically. Structure was treated with the SQUEEZE routine of PLATON6 as the highly disordered lattice CHCl3 solvent could not be suitably modelled. Residual e density: +1.153/-0.262 eÅ^{-3}. (ALERT B) Ratio of maximum / minimum residual density = 4.40; Q1 (+1.15 eÅ^{-3}) is on a center of inversion located between two complexes (see below, Q1-N1: 3.135 Å; Q1-N5: 2.903 Å) and may well be an artifact; Q2 is much lower (+0.39 eÅ^{-3}). SQUEEZE reported a void volume of 466 Å^3 per unit cell which contained 172 e$^-$. This is reasonably close to the expected volume[6] and e$^-$ counts per unit cell for 4CHCl$_3$, of 288 Å^3 and 232 e$^-$, respectively. As Z = 4 (for a general position in this space group), this is consistent with formulation as [Fe^{II}(**L^{2pyrimidine}**)$_2$(NCBH3)$_2$]·2CHCl$_3$, which is also in excellent agreement with the elemental analysis and TGA results on this sample (see the experimental section of the paper).

$[Fe^{II}(\mathbf{L^{4pyrimidine}})_2(NCS)_2]$ (**4**). (Figures 4 and S9) Half of this complex is in the asymmetric unit (other half generated by inversion). No solvent of crystallization. No disorder. All non-H atoms refined anisotropically. Residual e^- density +0.448/-0.383 $eÅ^{-3}$.

$[FeII(\mathbf{L^{4pyrimidine}})_2(NCSe)_2]$ (**5**). (Figure S10) Half of this complex is in the asymmetric unit (other half generated by inversion). No solvent of crystallization. No disorder. All non-H atoms refined anisotropically. Residual e^- density +0.477/-0.344 $eÅ^{-3}$.

$[FeII(\mathbf{L^{4pyrimidine}})_2(NCSe)_2]\cdot 2CH_3OH$ (**5**$\cdot 2CH_3OH$). (Figures 5 and S12) Half of this complex is in the asymmetric unit (other half generated by inversion). One lattice methanol molecule per asymmetric unit is disordered over two sites (0.50:0.50 for O30-C30:O40-C40, Figure S19 and S20) in the same region of space. (ALERT B) notes that the second part of the disordered methanol molecule (O40 C40) does not have any acceptor to form a hydrogen bond; however this was the best model found after attempting to model it (a) in different atom positions or (b) by inverting the atom positions. All non-H atoms refined anisotropically but those atoms belonging to the disordered solvent methanol molecules that were refined isotropically. Residual e^-density +1.576/-0.675 $eÅ^{-3}$. The first five Q peaks are (from 0.5 to 0.40 $eÅ^{-3}$) which is adjacent to the NCSe co-ligand.

Table S1. Crystallographic data for ligand $\mathbf{L^{4pyrimidine}}$ and compounds $[Fe^{II}(\mathbf{L^{2pyrimidine}})_2(NCS)_2]$ (**1**), $[Fe^{II}(\mathbf{L^{2pyrimidine}})_2(NCSe)_2]$ (**2**), $[Fe^{II}(\mathbf{L^{2pyrimidine}})_2(NCBH_3)_2]$ (**3**), $[Fe^{II}(\mathbf{L^{4pyrimidine}})_2(NCS)_2$ (**4**), $[Fe^{II}(\mathbf{L^{4pyrimidine}})_2(NCSe)_2]$ (5) and $[Fe^{II}(\mathbf{L^{4pyrimidine}})_2(NCSe)_2]\cdot 2CH_3OH$ (**5**$\cdot 2CH_3OH$) at 100 K.

	$\mathbf{L^{4pyrimidine}}$	**1**	**2**	**3** (SQUEEZE'd)	**4**	**5**	**5**$\cdot 2CH_3OH$
Temperature (K)	100(2)	100(2)	100(2)	100(2)	100(2)	100(2)	100(2)
Empirical formula	$C_{19}H_{15}N_5$	$C_{40}H_{30}N_{12}S_2Fe$	$C_{40}H_{30}N_{12}Se_2Fe$	$C_{40}H_{36}N_{12}B_2Fe$	$C_{40}H_{30}N_{12}S_2Fe$	$C_{40}H_{30}N_{12}Se_2Fe$	$C_{42}H_{38}N_{12}O_2Se_2Fe$
Mr	313.36	798.73	892.53	762.28	798.73	892.53	956.61
Crystal system	Monoclinic	Triclinic	Triclinic	Monoclinic	Monoclinic	Triclinic	Triclinic
Space group	P 21/n	P -1	P -1	P 21/n	P 21/n	P -1	P -1
a [Å]	5.5463(2)	8.9726(2)	9.0208(5)	11.265(2)	9.6929(8)	9.0098(5)	9.0029(2)
b [Å]	16.5747(4)	9.2240(5)	9.2522(7)	25.3945(7)	7.4970(4)	9.3563(6)	9.8087(4)
c [Å]	16.4664(5)	11.4261(6)	11.4631(6)	14.741(3)	25.051(2)	11.5968(7)	13.5703(4)
α [°]	90	76.541(4)	76.807(5)	90	90	75.804(6)	93.904(3)
β [°]	94.803(3)	75.658(3)	76.405(5)	148.66(4)	93.794(9)	75.291(5)	107.612(2)
γ [°]	90	85.953(3)	85.533(5)	90	90	84.400(5)	113.873(3)
V [Å^3]	1508.42(8)	890.95(7)	905.09(10)	2193(3)	1816.4(2)	916.03(10)	1019.20(6)
Z	4	1	1	2	2	1	1
$\rho_{calcd.}$ [Mg·m^3]	1.380	1.489	1.638	1.154	1.460	1.618	1.484
Wavelength [Å]	1.54184	0.71073	0.71073	1.54184	0.71073	0.71073	0.71073
μ [mm^{-1}]	0.690	0.591	2.478	3.081	0.580	2.448	2.203
F(000)	656	412	448	792	824	448	458
Crystal size [mm^3]	0.265 x 0.090 x 0.038	0.245 x 0.197 x 0.151	0.140 x 0.030 x 0.020	0.101 x 0.058 x 0.043	0.260 x 0.140 x 0.100	0.120 x 0.040 x 0.030	0.200 x 0.140 x 0.080
θ range: data collection [º]	3.791 to 73.386	3.170 to 26.021	3.158 to 26.022	3.481 to 72.129	3.120 to 26.020	3.10 to 26.02	2.84 to 26.02
Reflections collected	7358	28684	14578	10422	30217	14778	16377
Independent reflections	2959	3493	3548	4251	3566	3603	4009
R(int)	0.0567	0.0265	0.0578	0.0365	0.0267	0.0553	0.0483
Max./min. transmission	0.414 and 0.028	0.8687 and 0.9160	0.723 and 0.952	1 and 0.96917	0.944 and 0.864	0.9302 and 0.7577	0.915 and 0.831
Data/restraints / parameters	2959 / 0 / 217	3493 / 0 / 251	3548 / 0 / 251	4251 / 0 / 252	3566 / 0 / 250	3603 / 0 / 251	4009 / 2 / 269
Max/min e$^-$ density [eÅ^{-1}]	0.397 and -0.274	0.301 and -0.327	0.467 and -0.418	1.153 and -0.262	0.448 and -0.383	0.477 and -0.344	1.576 and -0.675
Goof (F^2)	1.052	1.094	1.070	1.132	1.181	1.033	1.098
R_1 / wR_2 [I>2σ(I)]	R1 = 0.0607, wR2 = 0.1603	R1 = 0.0260, wR2 = 0.0664	R1 = 0.0408, wR2 = 0.0885	R1 = 0.0605, wR2 = 0.1528	R1 = 0.0322, wR2 = 0.0867	R1 = 0.0375, wR2 = 0.0738	R1 = 0.0609, wR2 = 0.1758
wR_2 [all data]	0.1652	0.0668	0.0960	0.1571	0.0873	0.0795	0.1842

Table S2. Selected bond distances and angles in structures of compounds $[Fe^{II}(\mathbf{L^{2pyrimidine}})_2(NCS)_2]$ (**1**), $[Fe^{II}(\mathbf{L^{2pyrimidine}})_2(NCSe)_2]$ (**2**), $[Fe^{II}(\mathbf{L^{2pyrimidine}})_2(NCBH_3)_2]$ (**3**) (lattice solvent was treated by *SQUEEZE*), $[Fe^{II}(\mathbf{L^{4pyrimidine}})_2(NCS)_2]$ (**4**), $[Fe^{II}(\mathbf{L^{4pyrimidine}})_2(NCSe)_2]$ (**5**) and $[Fe^{II}(\mathbf{L^{4pyrimidine}})_2(NCSe)_2]\cdot 2CH_3OH$ (**5**$\cdot 2CH_3OH$) at 100 K.

Compound **1**		Compound **2**		Compound **3**$\cdot 2CHCl_3$		Compound **4**		Compound **5**		Compound **5**$\cdot 2CH_3OH$	
Fe1-N1 / Å	2.2286(13)	Fe1-N1 / Å	2.221(3)	Fe1-N1 / Å	2.007(4)	Fe1-N1 / Å	2.2352(15)	Fe1-N1 / Å	2.205(2)	Fe1-N1 / Å	2.190(3)
Fe1-N3 / Å	2.1859(13)	Fe1-N3 / Å	2.178(3)	Fe1-N3 / Å	1.953(4)	Fe1-N3 / Å	2.1574(15)	Fe1-N3 / Å	2.175(3)	Fe1-N3 / Å	2.179(3)
Fe1-N6 / Å	2.0915(14)	Fe1-N6 / Å	2.100(3)	Fe1-N6 / Å	1.926(6)	Fe1-N6 / Å	2.1002(15)	Fe1-N6 / Å	2.100(3)	Fe1-N6 / Å	2.111(3)
N1-Fe1-N3 / °	74.30(5)	N1-Fe1-N3 / °	74.22(10)	N1-Fe1-N3 / °	80.65(18)	N1-Fe1-N3 / °	74.45(5)	N1-Fe1-N3 / °	74.22(10)	N1-Fe1-N3 / °	75.91(11)
N1-Fe1-N3a / °	105.70(5)	N1-Fe1-N3a / °	105.28(10)	N1-Fe1-N3a / °	99.35(18)	N1-Fe1-N3a / °	105.56(5)	N1-Fe1-N3a / °	105.78(10)	N1-Fe1-N3a / °	104.09(11)
N3-Fe1-N1a / °	105.70(5)	N3-Fe1-N1a / °	105.28(10)	N3-Fe1-N1a / °	99.35(18)	N3-Fe1-N1a / °	105.56(5)	N3-Fe1-N1a / °	105.78(10)	N3-Fe1-N1a / °	104.09(11)
N6-Fe1-N1a / °	83.03(5)	N6-Fe1-N1a / °	83.21(11)	N6-Fe1-N1a / °	90.5(2)	N6-Fe1-N1a / °	92.79(6)	N6-Fe1-N1a / °	96.49(10)	N6-Fe1-N1a / °	89.48(12)
N1a-Fe1-N3a / °	74.30(5)	N1a-Fe1-N3a / °	74.72(10)	N1a-Fe1-N3a / °	80.65(18)	N1a-Fe1-N3a / °	74.45(5)	N1a-Fe1-N3a / °	74.22(10)	N1a-Fe1-N3a / °	75.91(11)
N1-Fe1-N6 / °	96.97(5)	N1-Fe1-N6 / °	96.79(11)	N1-Fe1-N6 / °	89.5(2)	N1-Fe1-N6 / °	87.21(6)	N1-Fe1-N6 / °	83.51(10)	N1-Fe1-N6 / °	90.52(12)
N1-Fe1-N6a / °	83.03(5)	N1-Fe1-N6a / °	83.21(11)	N1-Fe1-N6a / °	90.5(2)	N1-Fe1-N6a / °	92.79(6)	N1-Fe1-N6a / °	96.49(10)	N1-Fe1-N6a / °	89.48(12)
N3-Fe1-N3a / °	180.00	N3-Fe1-N3a / °	180.00	N3-Fe1-N3a / °	180.00	N3-Fe1-N3a / °	180.00	N3-Fe1-N3a / °	180.00	N3-Fe1-N3a / °	180.00
N6-Fe1-N3a / °	84.61(5)	N6-Fe1-N3a / °	85.26(10)	N6-Fe1-N3a / °	90.9(2)	N6-Fe1-N3a / °	91.09(6)	N6-Fe1-N3a / °	94.52(10)	N6-Fe1-N3a / °	96.77(10)
N1a-Fe1-N6a / °	96.97(5)	N1a-Fe1-N6a / °	96.79(11)	N1a-Fe1-N6a / °	89.5(2)	N1a-Fe1-N6a / °	87.21(6)	N1a-Fe1-N6a / °	83.51(10)	N1a-Fe1-N6a / °	90.52(12)
N1-Fe1-N1a / °	180.00	N1-Fe1-N1a / °	180.00	N1-Fe1-N1a / °	180.00	N1-Fe1-N1a / °	180.00	N1-Fe1-N1a / °	180.00	N1-Fe1-N1a / °	180.00
N3-Fe1-N6 / °	95.39(5)	N3-Fe1-N6 / °	94.74(10)	N3-Fe1-N6 / °	89.1(2)	N3-Fe1-N6 / °	88.91(6)	N3-Fe1-N6 / °	85.48(10)	N3-Fe1-N6 / °	83.23(10)
N3-Fe1-N6a / °	84.61(5)	N3-Fe1-N6a / °	85.26(10)	N3-Fe1-N6a / °	90.9(2)	N3-Fe1-N6a / °	91.09(6)	N3-Fe1-N6a / °	94.52(10)	N3-Fe1-N6a / °	96.77(10)
N6-Fe1-N6 / °	180.00	N6-Fe1-N6 / °	180.00	N6-Fe1-N6a / °	180.00	N6-Fe1-N6 / °	180.00	N6-Fe1-N6 / °	180.00	N6-Fe1-N6 / °	180.00
N3a-Fe1-N6a / °	95.39(5)	N3a-Fe1-N6a / °	94.74(10)	N3a-Fe1-N6a / °	89.1(2)	N3a-Fe1-N6a / °	88.91(6)	N3a-Fe1-N6a / °	85.48(10)	N3a-Fe1-N6a / °	83.23(10)

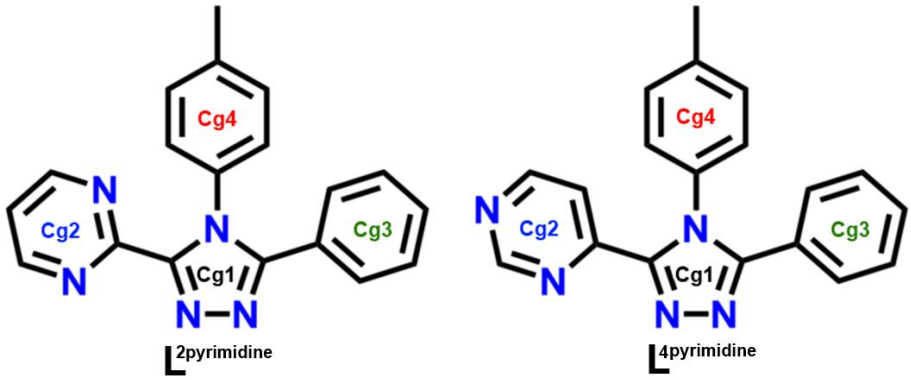

Figure S5. Schematic representation of ligands $\mathbf{L}^{\mathbf{2pyrimidine}}$ and $\mathbf{L}^{\mathbf{4pyrimidine}}$ showing each ring and its corresponding centroid. Centroid color code: triazole ring is Cg1 (black), pyrimidine ring is Cg2 (blue), phenyl ring is Cg3 (green), and tolyl ring is Cg4 (red).

Table S3. Selected intra-, and intermolecular contacts in the structure of compound $[Fe^{II}(\mathbf{L}^{\mathbf{2pyrimidine}})_2(NCS)_2]$ (**1**) at 100 K.

Compound $[Fe^{II}(\mathbf{L}^{\mathbf{2pyrimidine}})_2(NCS)_2]$ (**1**)				
D-H…A	D-H / Å	H…A / Å	D…A / Å	D-H…A / °
C8-H8…N5 *(intra)*	0.95	2.45	2.7981(2)	102
C18-H18…N5	0.95	2.42	3.3227(19)	158
Centroid…Centroid		Cg…Cg / Å		α / º
Cg1-Cg1		3.7367(9)		0.03(8)
Cg1-Cg3		4.7420(9)		7.62(8)
Cg1-Cg3		4.6557(9)		7.62(8)
Cg2-Cg3		3.9926(9)		16.34(9)
Cg3-Cg3		3.9313(10)		0.02(8)
X-H…Centroid		H…Cg / Å	X…Cg / Å	X-H…Cg / °
C12-H12…Cg4 *(intra)*		2.68	3.5716(17)	157
NCS…SCN			S…S / Å	
S1…S1A			3.644	

Table S4. Selected intra-, and intermolecular contacts in the structure of compound $[Fe^{II}(\mathbf{L^{2pyrimidine}})_2(NCSe)_2]$ (**2**) at 100 K.

Compound $[Fe^{II}(\mathbf{L^{2pyrimidine}})_2(NCSe)_2]$ (**2**)				
D-H…A	D-H / Å	H…A / Å	D…A / Å	D-H…A / °
C8-H8…N5 *(intra)*	0.95	2.45	2.801(5)	101
C18-H18…N5	0.95	2.45	3.362(4)	161
Centroid…Centroid		Cg…Cg / Å		α / º
Cg1-Cg1		3.8147(18)		0.03(19)
Cg1-Cg3		4.744(2)		10.83(18)
Cg1-Cg3		4.682((2)		10.83(18)
Cg2-Cg3		4.097(2)		19.99(17)
Cg3-Cg3		3.951(2)		0.00(17)
X-H…Centroid		H…Cg / Å	X…Cg / Å	X-H…Cg / °
C12-H12…Cg4 *(intra)*		2.71	3.597(4)	41
NCSe…SeCN			Se…Se / Å	
Se1…Se1A			3.475	

Table S5. Selected intra-, and intermolecular contacts in the structure of compound $[Fe^{II}(\mathbf{L^{2pyrimidine}})_2(NCBH_3)_2]$ (**3**) at 100 K.

Compound $[Fe^{II}(\mathbf{L^{2pyrimidine}})_2(NCBH_3)_2]\cdot 2CHCl_3$ (**3**·2CHCl$_3$; note that the lattice solvent was treated by SQUEEZE[7])				
D-H…A	D-H / Å	H…A / Å	D…A / Å	D-H…A / °
C1-H1…N5 *(intra)*	0.95	2.32	3.111(9)	141
C17-H17…N2	0.95	2.712	3.606(9)	157
C2-H2…B1	0.95	3.064	3.826(9)	138
C14-H14…B1	0.95	3.091	3.700(9)	123
C10-H10…B1	0.95	3.017	3.902(9)	156
Centroid…Centroid		Cg…Cg / Å		α / º
Cg1-Cg2		4.919(3)		5.2(3)
Cg1-Cg3		4.750(4)		42.3(3)
Cg2-Cg3		4.618(5)		39.6(3)
Cg3-Cg3		4.296(3)		0.0(2)
Cg4-Cg4		4.730(2)		19.8(2)
X-H…Centroid		H…Cg / Å	X…Cg / Å	X-H…Cg / °
C8-H8…Cg2		2.93	3.526(9)	122

Table S6. Selected intra-, and intermolecular contacts in the structure of compound $[Fe^{II}(\mathbf{L^{4pyrimidine}})_2(NCS)_2]$ (**4**) at 100 K.

Compound $[Fe^{II}(\mathbf{L^{4pyrimidine}})_2(NCS)_2]$ (**4**)				
D-H…A	D-H / Å	H…A / Å	D…A / Å	D-H…A / °
C8-H8…N5 *(intra)*	0.95	2.48	2.814(2)	101
Centroid…Centroid		Cg…Cg / Å		α / º
Cg1-Cg2		4.3356(10)		6.83(9)
Cg1-Cg3		4.6945(10)		15.21(9)
Cg2-Cg3		3.6634(10)		14.02(8)
X-H…Centroid		H…Cg / Å	X…Cg / Å	X-H…Cg / °
C12-H12…Cg4 *(intra)*		2.77	3.6193(18)	149
Y-X…Centroid		X…Cg / Å	Y…Cg / Å	Y-X…Cg / °
C20-S1…Cg4		3.9413(9)	4.1121(18)	84.21(6)

Table S7. Selected intra-, and intermolecular contacts in the structure of compound $[Fe^{II}(\mathbf{L^{4pyrimidine}})_2(NCSe)_2]$ (**5**) at 100 K.

$[Fe^{II}(\mathbf{L^{4pyrimidine}})_2(NCSe)_2]$ (**5**)				
D-H…A	D-H / Å	H…A / Å	D…A / Å	D-H…A / °
C8-H8…N5 *(intra)*	0.95	2.45	2.808(4)	102
C14-H14…N5	0.95	2.44	3.357(4)	163
Centroid…Centroid		Cg…Cg / Å		α / º
Cg1-Cg1		3.8337(18)		0.03(8)
Cg1-Cg3		4.7657(18)		7.65(16)
Cg1-Cg3		4.7594(18)		7.65(16)
Cg2-Cg3		4.0944(19)		16.81(15)
Cg3-Cg3		4.0002(19)		0.02(15)
X-H…Centroid		H…Cg / Å	X…Cg / Å	X-H…Cg / °
C3-H3…Cg4		2.92	3.747(4)	146
C12-H12…Cg4 *(intra)*		2.74	3.633(3)	156
NCSe…SeCN			Se…Se / Å	
Se1…Se1A			3.486	

Table S8. Selected intermolecular contacts in the structure of compound $[Fe^{II}(\mathbf{L}^{4pyrimidine})_2(NCSe)_2]\cdot 2CH_3OH$ ($\mathbf{5}\cdot 2CH_3OH$) at 100 K.

$[Fe^{II}(\mathbf{L}^{4pyrimidine})_2(NCSe)_2]\cdot 2CH_3OH$ ($\mathbf{5}\cdot 2CH_3OH$)				
D-H…A	D-H / Å	H…A / Å	D…A / Å	D-H…A / °
O30-H30X…N2	0.91	2.18	3.086(9)	172
C9-H9…N6	0.95	2.58	3.459(5)	154
C18-H18…O30	0.95	2.45	3.342(9)	157
C30-H30C…N6	0.98	2.61	3.491(18)	149
C40-H40B…N4	0.98	2.51	3.392(10)	149
X-H…Centroid		H…Cg / Å	X…Cg / Å	X-H…Cg / °
C19-H19B…Cg3		2.66	3.562(4)	154
C30-H30B…Cg1		2.63	3.505(17)	124
C40-H40B…Cg1		2.33	3.485(10)	145
Y-X…Centroid		X…Cg / Å	Y…Cg / Å	Y-X…Cg / °
C20-Se20…Cg4		3.9225(14)	5.621(4)	158.50(13)

S2.2. Crystal structure representations

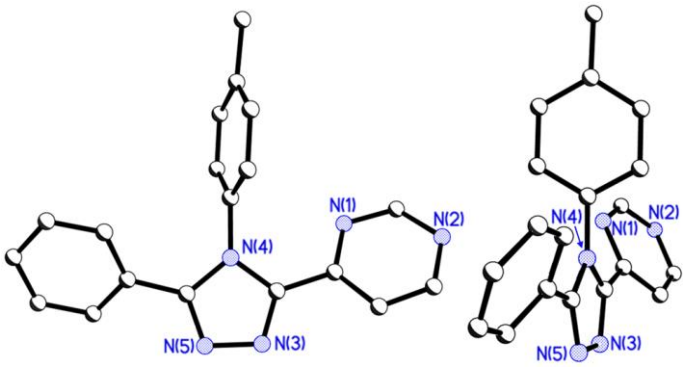

Figure S6. Two different perspective views of the structure of $\mathbf{L}^{4pyrimidine}$ at 100 K. (Left) with the triazole ring in the plane of the page and (right) with the phenyl ring in the plane of the page. Hydrogen atoms are omitted for clarity. Atom color code: nitrogen (blue) and carbon (black).

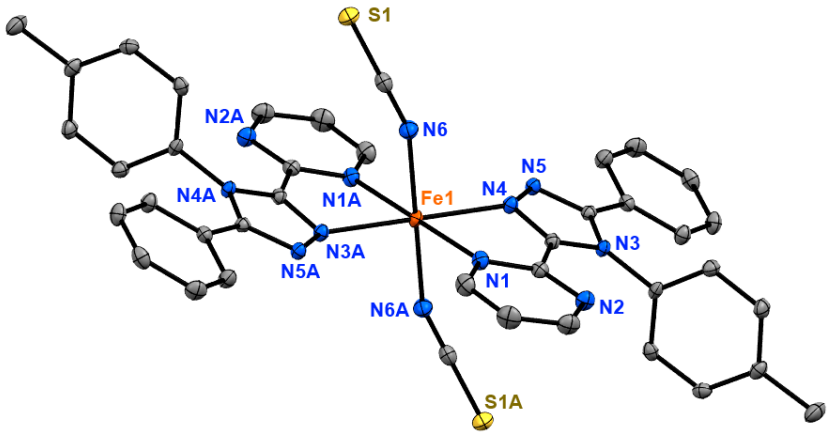

Figure S7. ORTEP representation (50% probability ellipsoids) of complex [Fe^{II}($L^{2pyrimidine}$)$_2$(NCS)$_2$] (**1**) at 100 K. Hydrogen atoms are omitted for clarity. Color atom code: iron(II) (orange), nitrogen (blue), sulfur (brown) and carbon (grey). Symmetry operation A is 1-x, 1-y, 1-z.

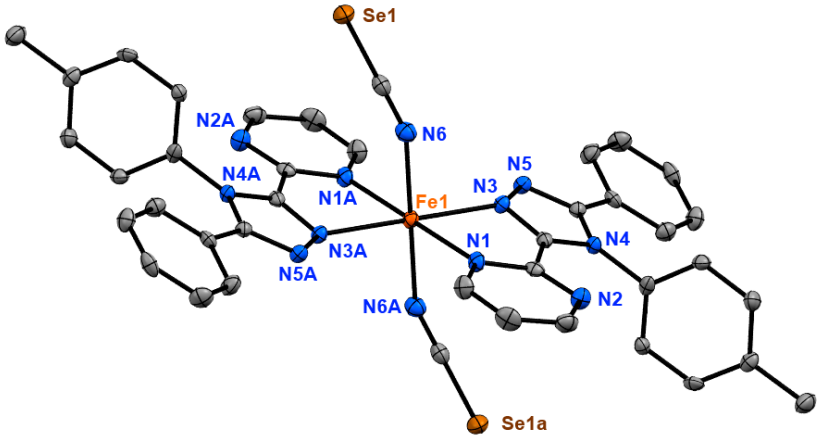

Figure S8. ORTEP representation (50% probability ellipsoids) of complex [Fe^{II}($L^{2pyrimidine}$)$_2$(NCSe)$_2$] (**2**) at 100 K. Hydrogen atoms are omitted for clarity. Color atom code: iron(II) (orange), nitrogen (blue), selenium (brown) and carbon (grey). Symmetry operation A is 2-x, -y, 1-z.

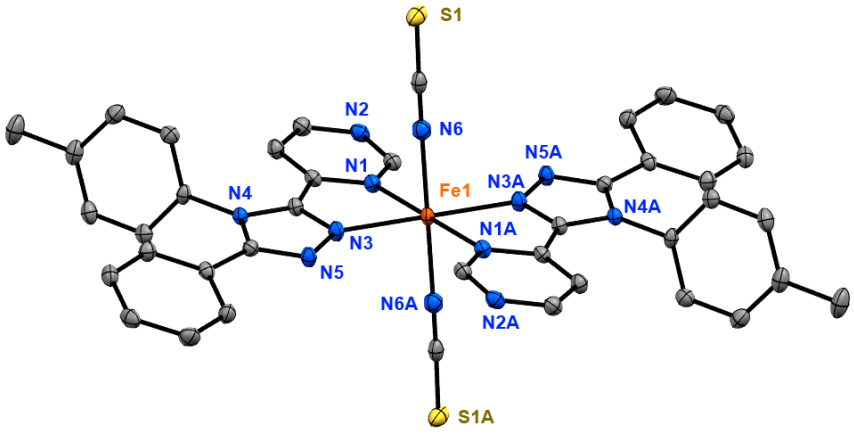

Figure S9. ORTEP representation (50% probability ellipsoids) of complex [Fe^{II}($L^{4pyrimidine}$)$_2$(NCS)$_2$] (**4**) at 100 K. Hydrogen atoms are omitted for clarity. Color atom code: iron(II) (orange), nitrogen (blue), sulfur (yellow) and carbon (grey). Symmetry operation A is 1-x, 1-y, 1-z.

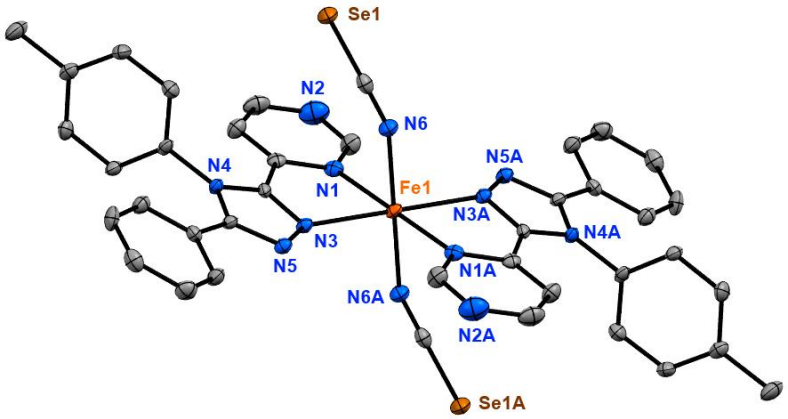

Figure S10. ORTEP representation (50% probability ellipsoids) of complex $[Fe^{II}(\mathbf{L}^{4pyrimidine})_2(NCSe)_2]$ (**5**) at 100 K. Hydrogen atoms are omitted for clarity. Color atom code: iron(II) (orange), nitrogen (blue), selenium (brown) and carbon (grey). Symmetry operation A is 2-x, 2-y, -z.

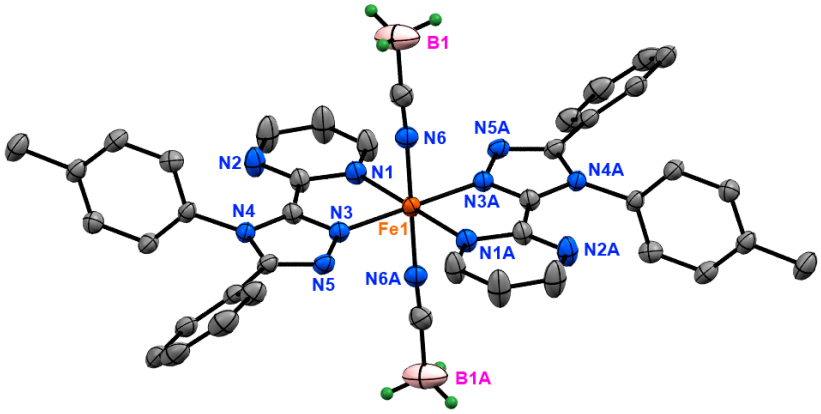

Figure S11. ORTEP representation (50% probability ellipsoids) of complex $[Fe^{II}(\mathbf{L}^{2pyrimidine})_2(NCBH_3)_2]\cdot 2CHCl_3$ (**3**·2$CHCl_3$; note that the lattice solvent was treated by SQUEEZE[7]) at 100 K. Hydrogen atoms are omitted for clarity, except those that belong to $NCBH_3$ co-ligands (green). Color atom code: iron(II) (orange), nitrogen (blue), boron (fuchsia) and carbon (grey). Symmetry operation A is -x, 1-y, 1-z.

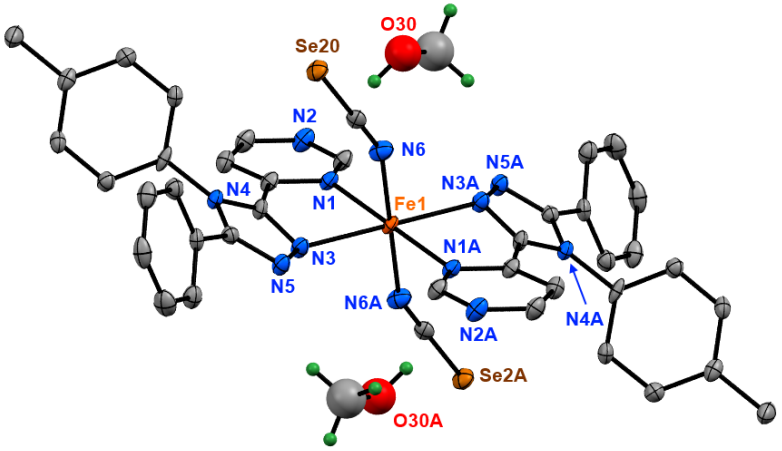

Figure S12. ORTEP representation (50% probability ellipsoids) of complex $[Fe^{II}(\mathbf{L}^{4pyrimidine})_2(NCSe)_2]\cdot 2CH_3OH$ (**5**·2CH_3OH) at 100 K. Only one of the two half occupancy methanol molecules per asymmetric unit is shown (O30-C30). Hydrogen atoms are omitted for clarity, except those in the lattice methanol molecules (green). Color atom code: iron(II) (orange), nitrogen (blue), selenium (brown), oxygen (red) and carbon (grey). Symmetry operation A is 1-x, 2-y, 1-z.

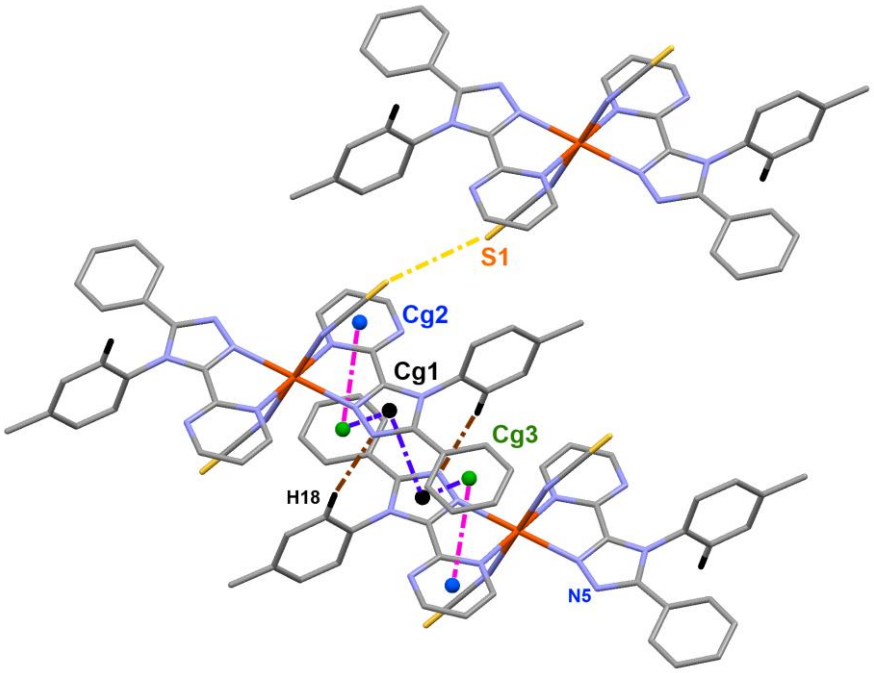

Figure S13. Perspective view of some intermolecular interactions in $[Fe^{II}(\mathbf{L}^{\mathbf{2pyrimidine}})_2(NCS)_2]$ (1). The two molecules (middle and bottom) in adjacent layers are connected by weak, non-classical C–H···N hydrogen bonds (brown dashed lines) and π···π (pink and purple dashed lines) interactions. The third molecule (top) is connected to the adjacent complex molecule (middle) through a S···S interaction (yellow dashed lines). Hydrogen atoms are omitted for clarity but those taking part in an intermolecular interaction (black). Note that the contacts in complexes **2** and **5** show the same type of contacts (Table S4 and S7, respectively) as complex **1**.

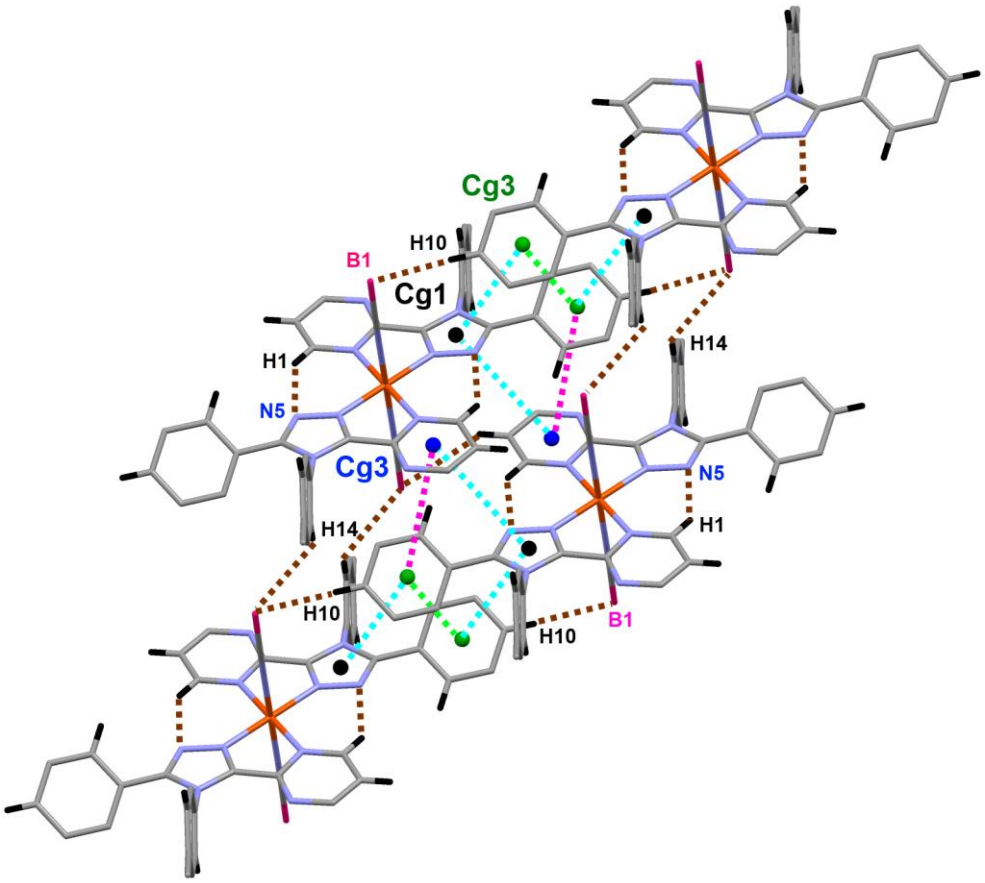

Figure S14. Perspective view of some intermolecular interactions in $[Fe^{II}(\mathbf{L}^{\mathbf{2pyrimidine}})_2(NCBH3)_2]\cdot 2CHCl_3$ (**3**·2CHCl3; note that the lattice solvent was treated by SQUEEZE6) at 100 K. The complexes in the crystal lattice are organized in ABAB layers (see figure S15). All shown molecules belong to the same layer and within each layer the complexes interact through π···π contacts (Cg1···Cg2 and Cg1···Cg3, light blue; Cg2···Cg3, fuchsia; Cg3···Cg3, light green) and CH···B contacts (brown). Hydrogen atoms are omitted for clarity except those taking part in an intermolecular contact (black).

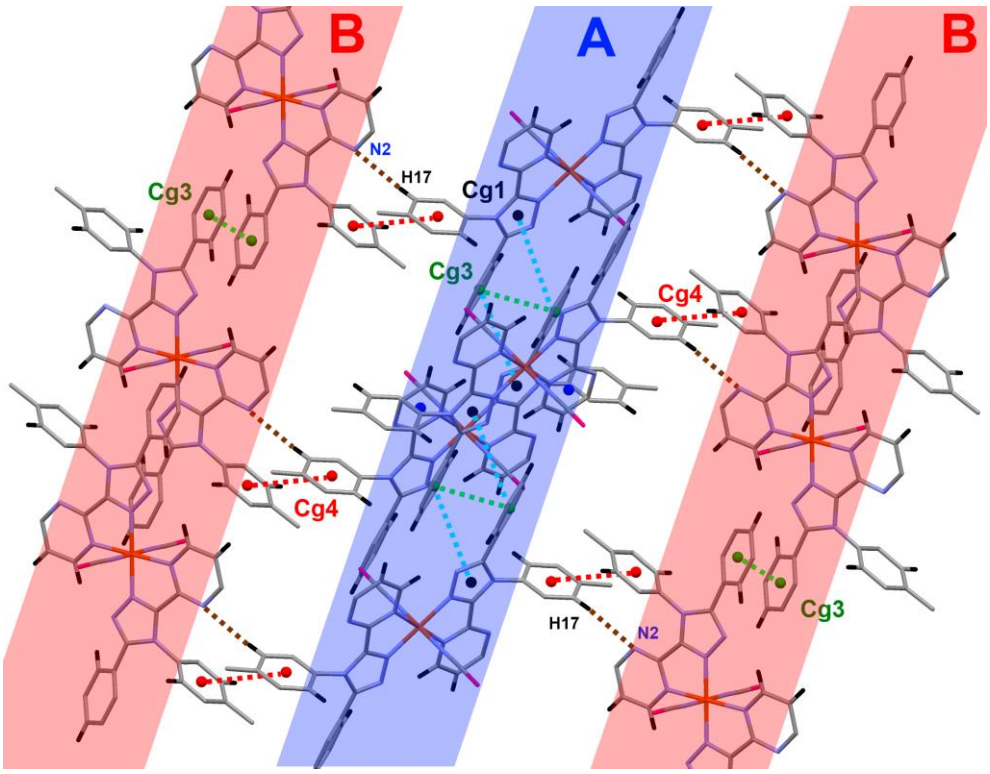

Figure S15. Perspective view of some intermolecular interactions in $[Fe^{II}(\mathbf{L}^{2pyrimidine})_2(NCBH_3)_2]\cdot 2CHCl_3$ (**3**·2$CHCl_3$; note that the lattice solvent was treated by SQUEEZE[7]) at 100 K. The complexes are organized in ABAB layers. The A layer (blue) corresponds to the same molecules shown in Figure S14. Molecules from adjacent layers interact through π···π contacts between tolyl rings (Cg4···Cg4, red) and CH···N contacts between the uncoordinated nitrogen N(2) atom and the tolyl rings (brown). Note that not all of the intermolecular contacts in the A layer (blue) are shown for clarity. Hydrogen atoms are omitted for clarity except those taking part in an intermolecular contact (black).

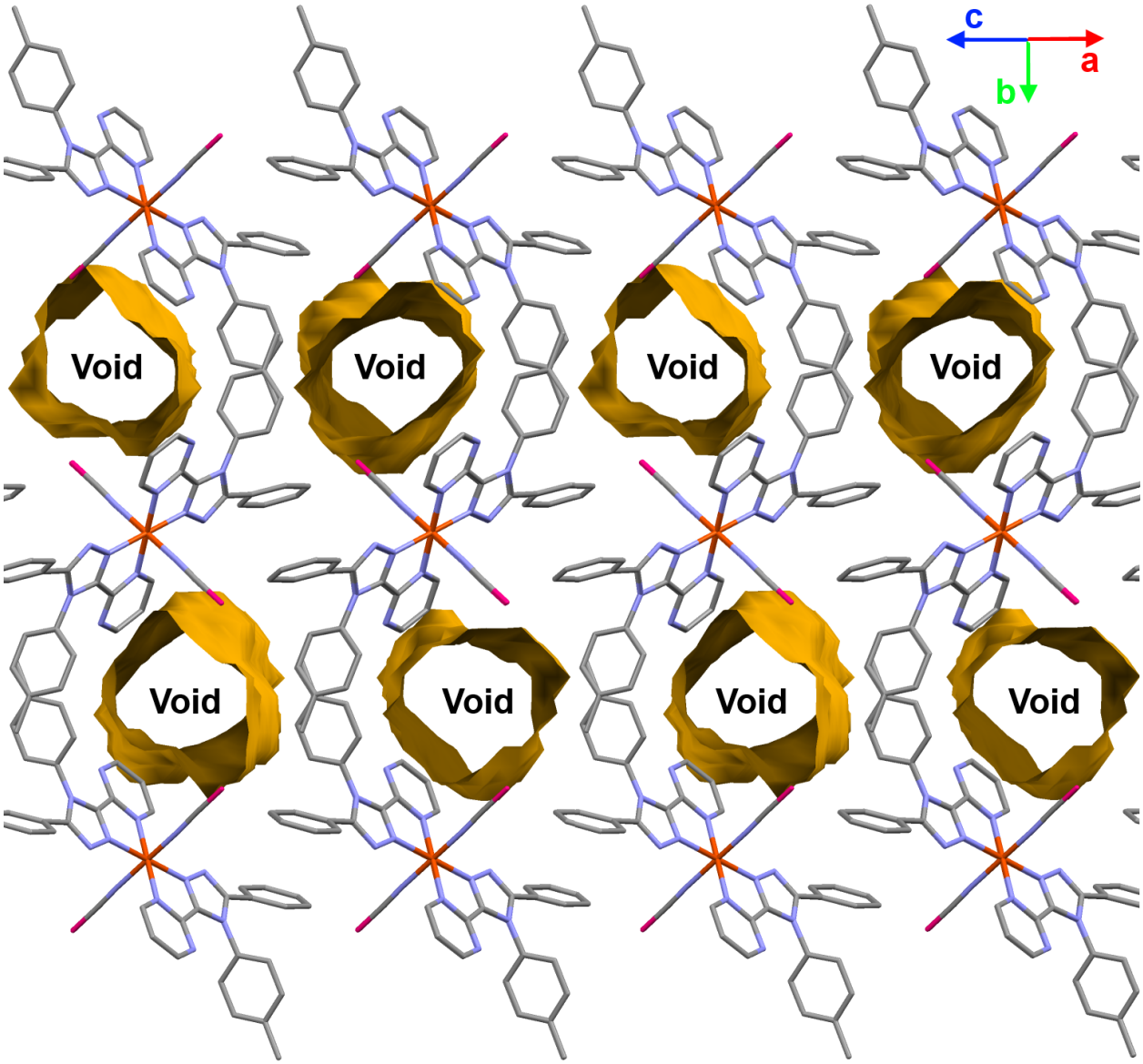

Figure S16. Edge on view of molecules of $[Fe^{II}(\mathbf{L}^{2pyrimidine})_2(NCBH_3)_2]\cdot 2CHCl_3$ (**3**·2$CHCl_3$; note that the lattice solvent was treated by SQUEEZE[7]) at 100 K showing the voids where disordered lattice $CHCl_3$ could be found before using *SQUEEZE*. Note that the voids are located in the tolyl region between adjacent layers of complexes - a feature also seen in analogous systems.[8-9]

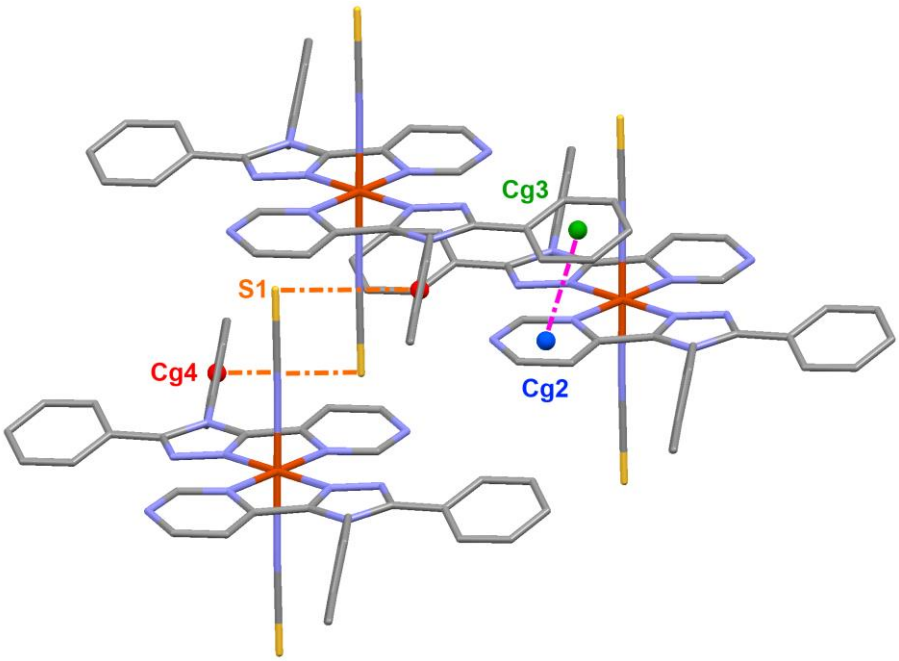

Figure S17. Perspective view of the π···π (pink dashed lines) and NCS···π interactions (orange dashed lines) between adjacent complexes in $[Fe^{II}(\mathbf{L}^{4pyrimidine})_2(NCS)_2]$ (**4**).

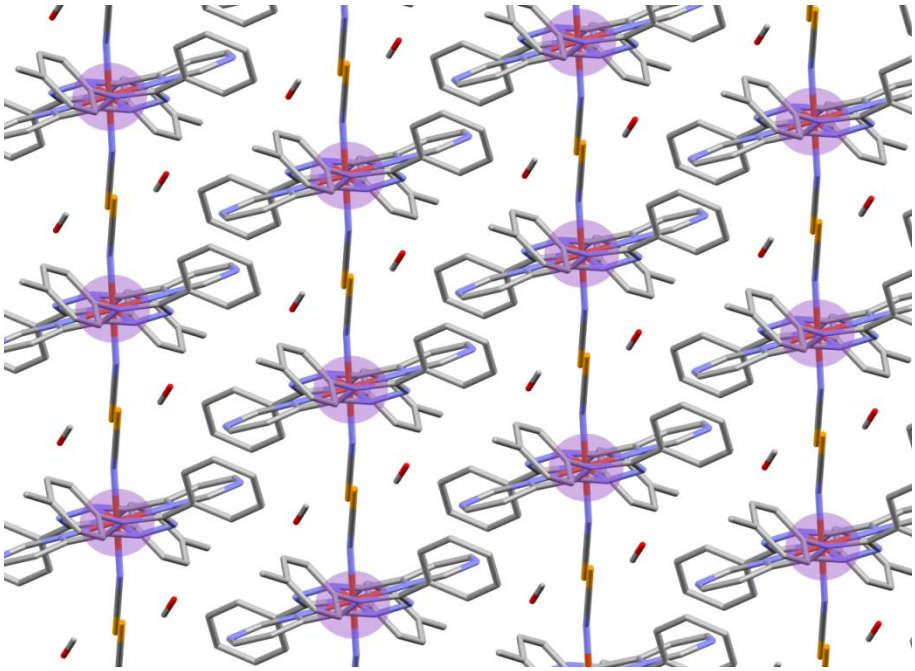

Figure S18. Perspective view of the complex $[Fe^{II}(\mathbf{L}^{4pyrimidine})_2(NCSe)_2]\cdot 2CH_3OH$ (**5**·$2CH_3OH$) looking along the (011) plane following the wave-like layers (purple highlight) into the page. The compound arranges with alternating complex/solvent in two directions. Hydrogen atoms and one of the two half occupancy methanol molecules are omitted for clarity.

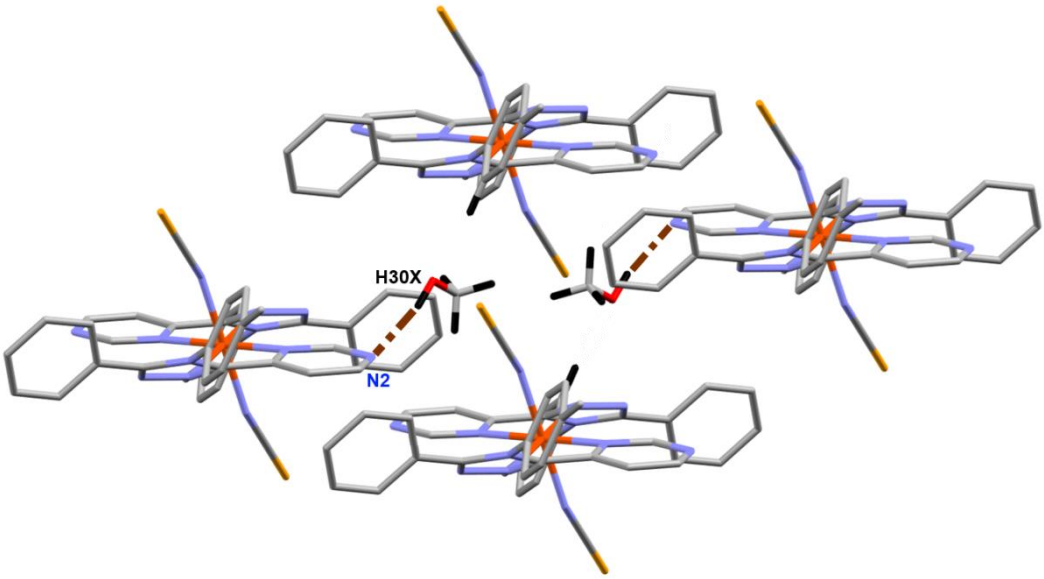

Figure S19. Perspective view of the solvent interactions involving one of the two half occupancy methanol molecules, (O30–C30, in the $[Fe^{II}(\mathbf{L}^{4pyrimidine})_2(NCSe)_2]\cdot 2CH_3OH$ (**5**·$2CH_3OH$) complex. Each O30–C30 methanol molecule interacts with one complex molecule via a hydrogen bonds (brown dashed lines). Hydrogen atoms are omitted for clarity but those taking part in a contact.

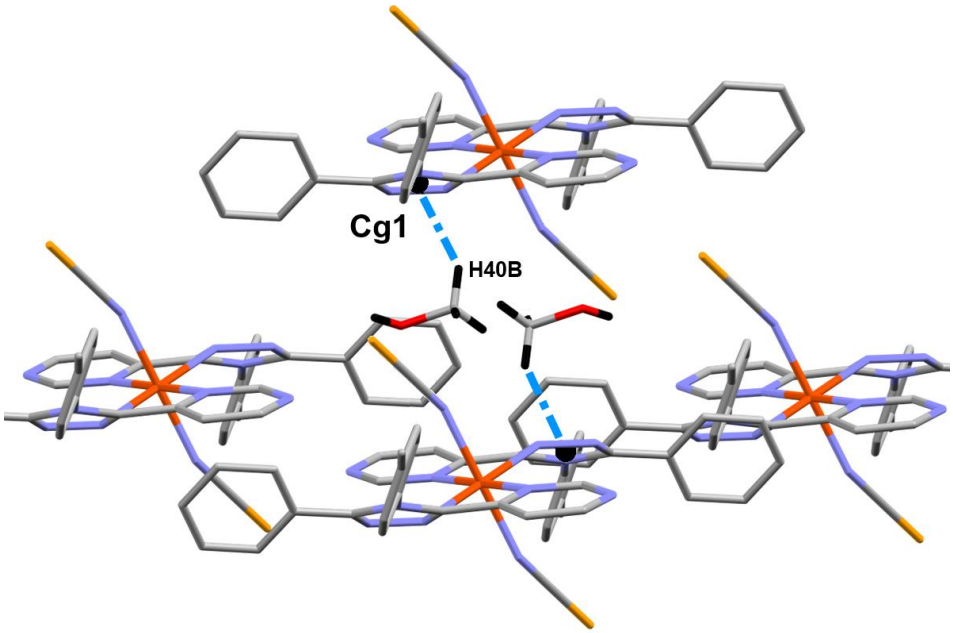

Figure S20. Perspective view of the solvent interactions involving the other of the two half occupancy methanol molecules, C(40)–O(40), in the $[Fe^{II}(\mathbf{L}^{4pyrimidine})_2(NCSe)_2]\cdot 2CH_3OH$ (**5**·$2CH_3OH$) complex. Each solvent molecule is connected to one molecule of complex through C–H···π interactions (light blue dashed lines). Hydrogen atoms that do not take part in intermolecular contacts and the partial occupancy methanol (O(30)–C(30)) (see Figure S12) are omitted for clarity.

S3. Solid state magnetic measurement

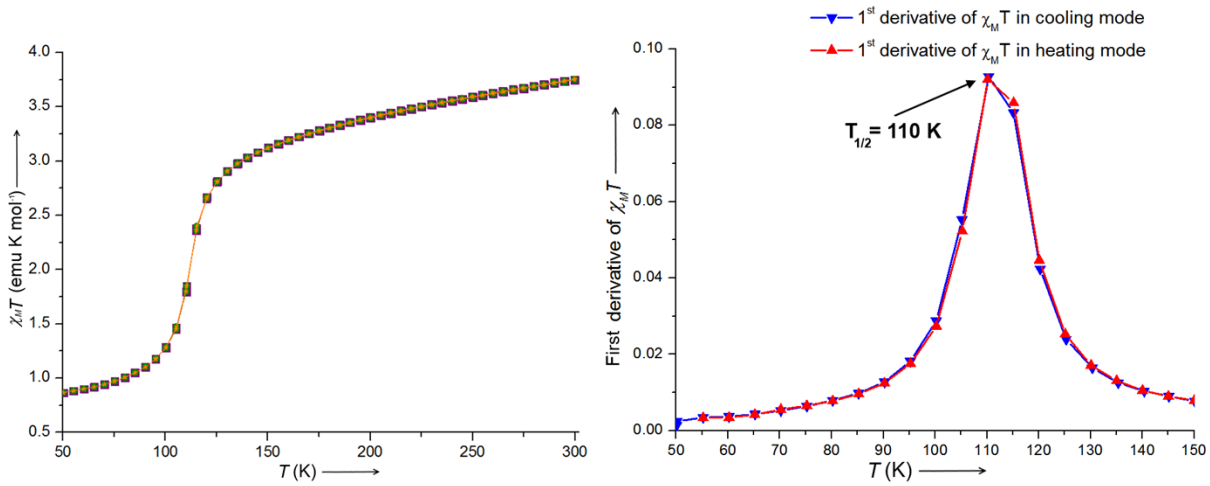

Figure S21. (Left) Plot $\chi_M T$ vs T showing three cooling-heating cycles from 50 to 300 K at 2 K·min^{-1} on settle mode for compound [Fe^{II}(**L**^{4pyrimidine})$_2$(NCSe)$_2$]·1.5H$_2$O (**5**·1.5H$_2$O). $T_{1/2}$ = 110 K. Colour code: first cycle (orange stars), second cycle (green circles) and third cycle (purple squares). (Right) Second derivative of $\chi_M T$ vs T for **5**·1.5H$_2$O confirming that $T_{1/2}$ =110 K (cooling mode, blue triangles; warming mode, red triangles).

S4. UV-Vis spectroscopy

S4.1. UV-Vis spectra of $L^{npyrimidine}$ ligands

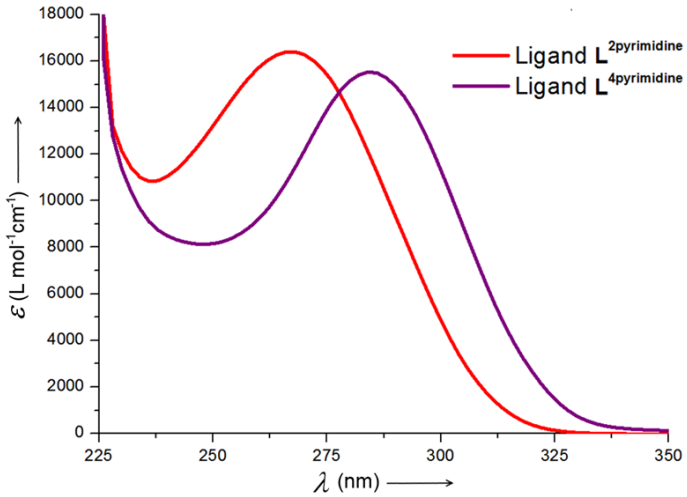

Figure S22. UV-VIS spectra of free ligand $\mathbf{L^{2pyrimidine}}$ (red, $5{\cdot}10^{-5}$ M) and $\mathbf{L^{4pyrimidine}}$ (purple, $5{\cdot}10^{-5}$ M) in $CHCl_3$. Note that this figure is taken from ref. [10] and is shown here simply to facilitate comparisons between both ligands.

S4.2. UV-Vis spectra of $[Fe^{II}(L^{npyrimidine})_2(NCBH_3)_2]$ complexes in CH_2Cl_2

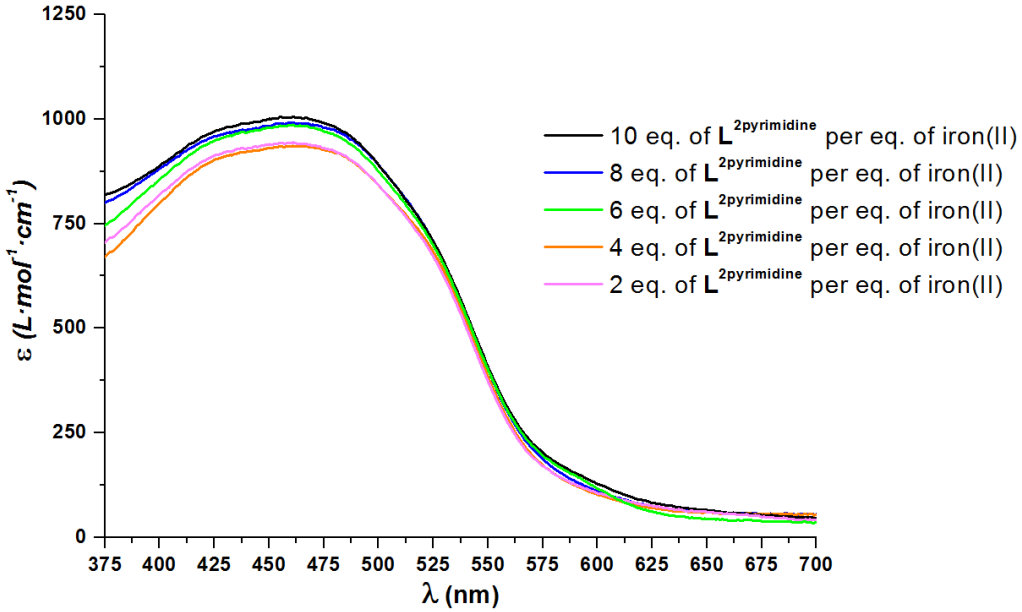

Figure S23. UV-Vis spectra of the speciation study of compound $[Fe^{II}(\mathbf{L^{2pyrimidine}})_2(NCBH_3)_2]$ in CH_2Cl_2 using different $\mathbf{L^{2pyrimidine}}/Fe^{II}$ ratios.

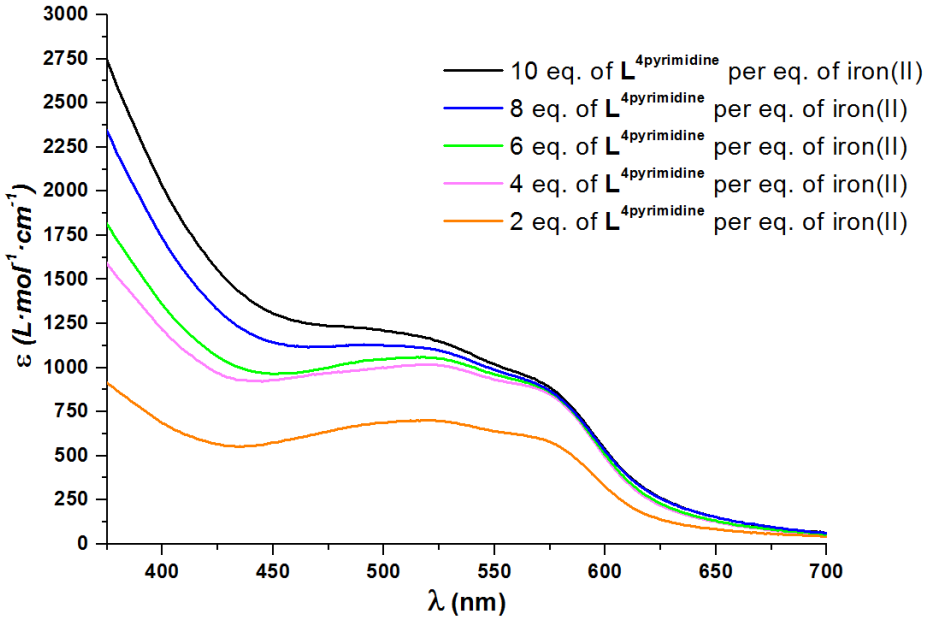

Figure S24. UV-Vis spectra of the speciation study of compound $[Fe^{II}(\mathbf{L^{4pyrimidine}})_2(NCBH_3)_2]$ in CH_2Cl_2 using different $\mathbf{L^{4pyrimidine}}/Fe^{II}$ ratios.

S4.3. UV-Vis spectra of $[Fe^{II}(L^{npyrimidine})_2(NCBH_3)_2]$ complexes in $CHCl_3$

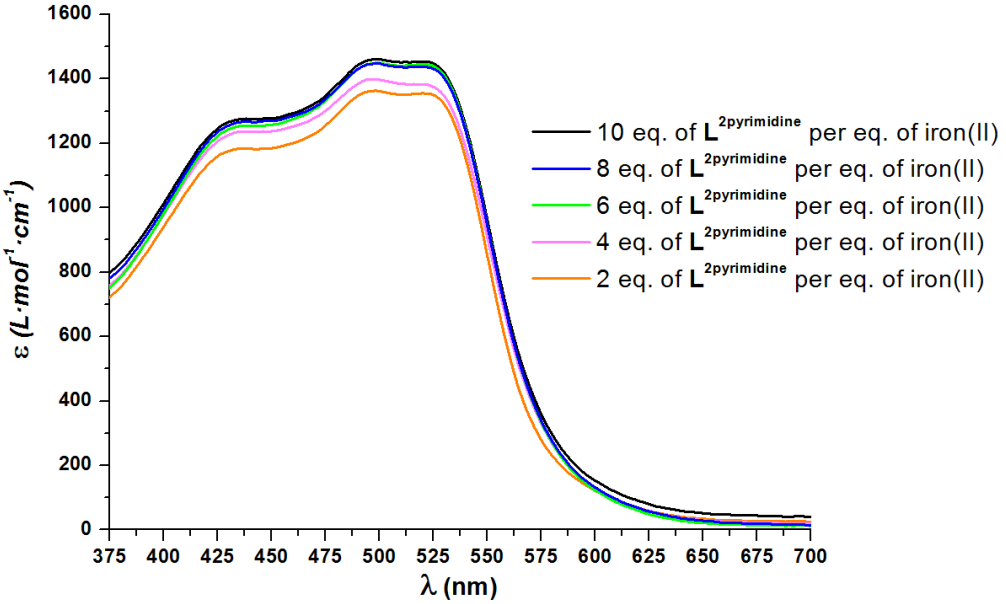

Figure S25. UV-Vis spectra of the speciation study of compound $[Fe^{II}(\mathbf{L^{2pyrimidine}})_2(NCBH_3)_2]$ in $CHCl_3$ using different $\mathbf{L^{2pyrimidine}}/Fe^{II}$ ratios. Note that this figure is taken from ref. [10] and is shown here simply to facilitate comparison with the different UV-vis spectra in other solvents.

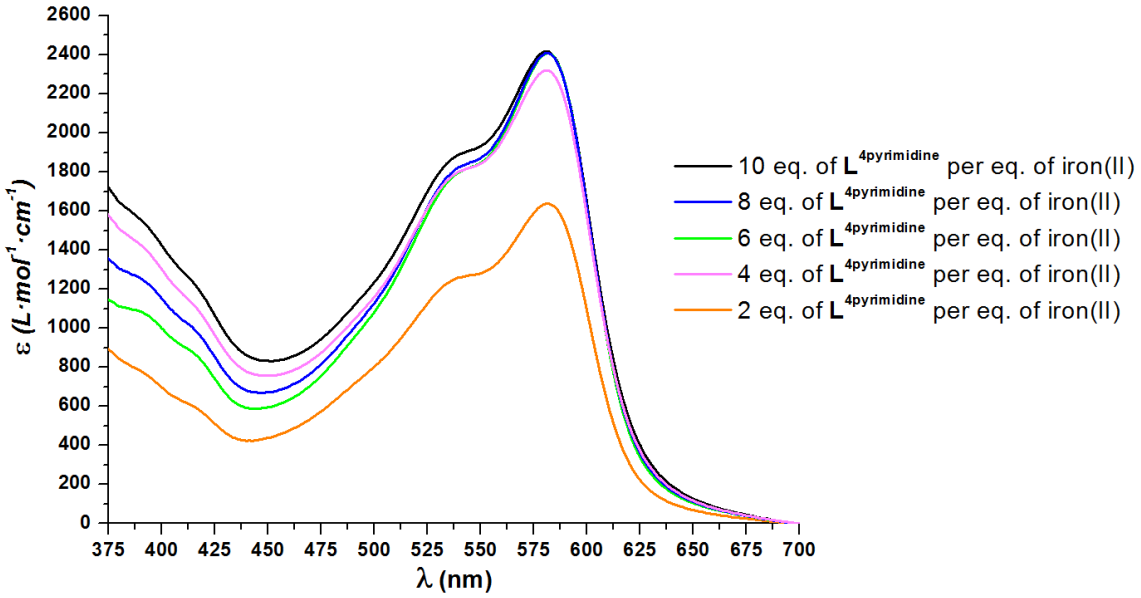

Figure S26. UV-Vis spectra of the speciation study of compound $[Fe^{II}(\mathbf{L^{4pyrimidine}})_2(NCBH_3)_2]$ in $CHCl_3$ using different $\mathbf{L^{4pyrimidine}}/Fe^{II}$ ratios. Note that this figure is taken from ref. [10] and is shown here simply to facilitate comparison with the different UV-vis spectra in other solvents.

S4.4. UV-Vis spectra of $[Fe^{II}(L^{n\text{pyrimidine}})_2(NCBH_3)_2]$ complexes in $(CH_3)_2CO$

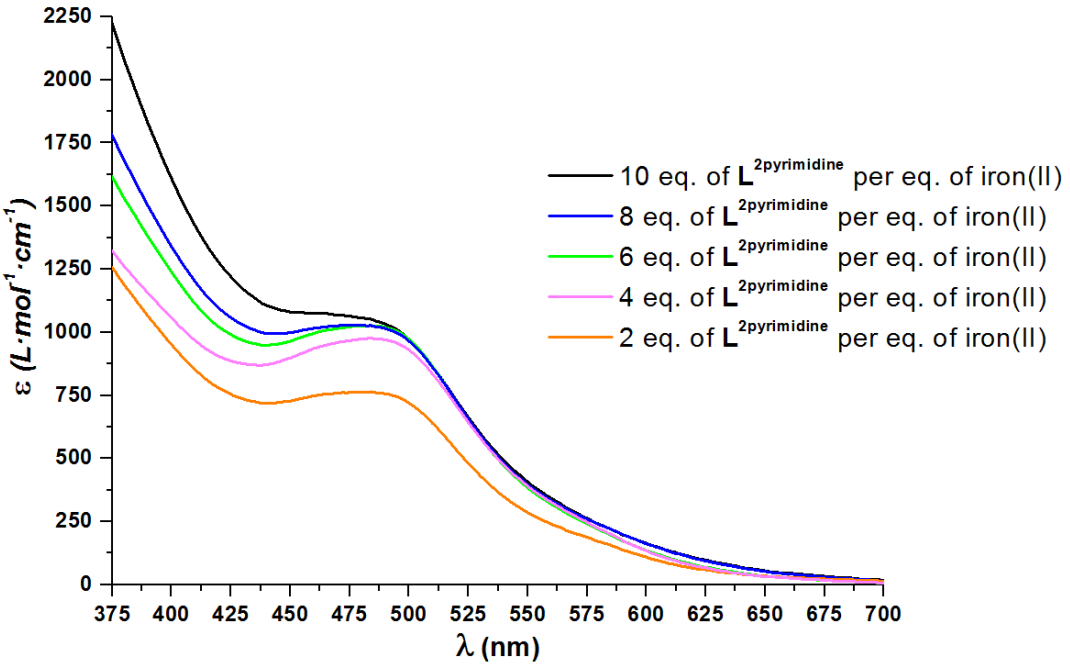

Figure S27. UV-Vis spectra of the speciation study of compound $[Fe^{II}(\mathbf{L^{2pyrimidine}})_2(NCBH_3)_2]$ in $(CH_3)_2CO$ using different $\mathbf{L^{4pyrimidine}}/Fe^{II}$ ratios.

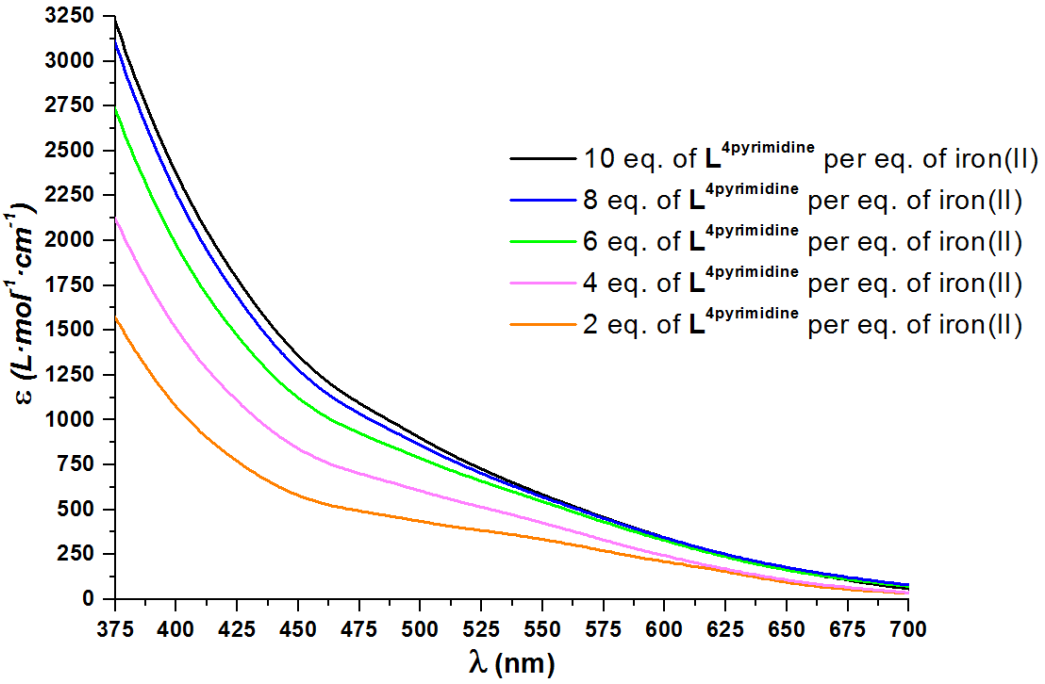

Figure S28. UV-Vis spectra of the speciation study of compound $[Fe^{II}(\mathbf{L^{4pyrimidine}})_2(NCBH_3)_2]$ in $(CH_3)_2CO$ using different $\mathbf{L^{4pyrimidine}}/Fe^{II}$ ratios.

S4.5. UV-Vis spectra of $[Fe^{II}(L^{npyrimidine})_2(NCBH_3)_2]$ complexes in CH_3CN

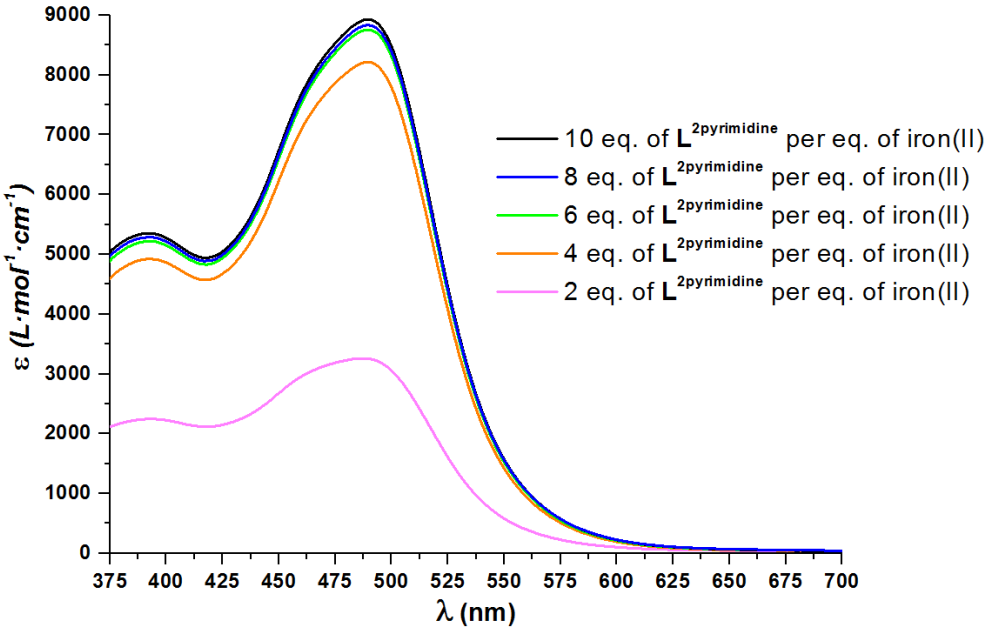

Figure S29. UV-Vis spectra of the speciation study of compound $[Fe^{II}(\mathbf{L^{2pyrimidine}})_2(NCBH_3)_2]$ in CH_3CN using different $\mathbf{L^{2pyrimidine}}/Fe^{II}$ ratios.

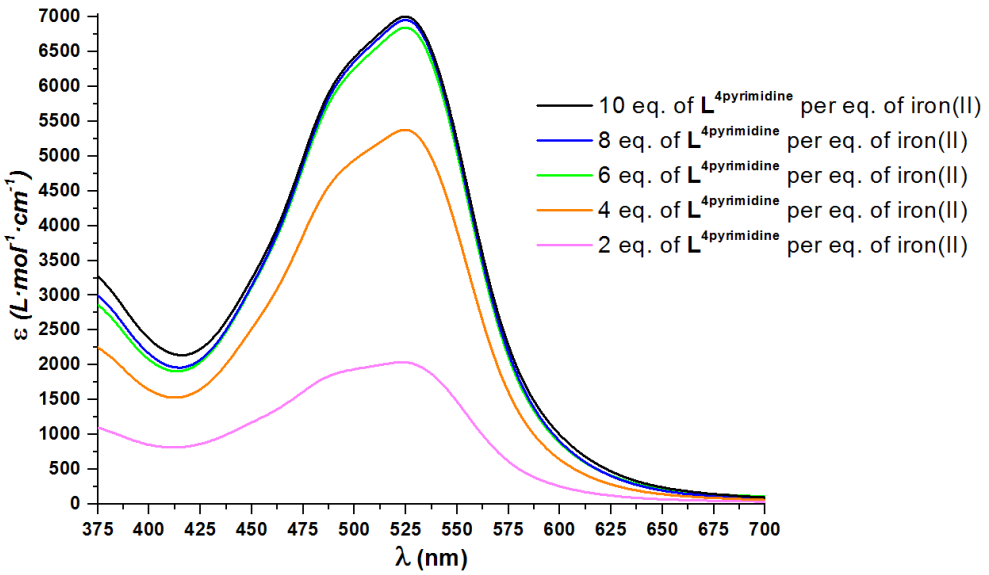

Figure S30. UV-Vis spectra of the speciation study of compound $[Fe^{II}(\mathbf{L^{4pyrimidine}})_2(NCBH_3)_2]$ in CH_3CN using different $\mathbf{L^{2pyrimidine}}/Fe^{II}$ ratios.

S4.6. UV-Vis spectra of $[Fe^{II}(L^{n\text{pyrimidine}})_2(NCBH_3)_2]$ complexes in CH_3NO_2

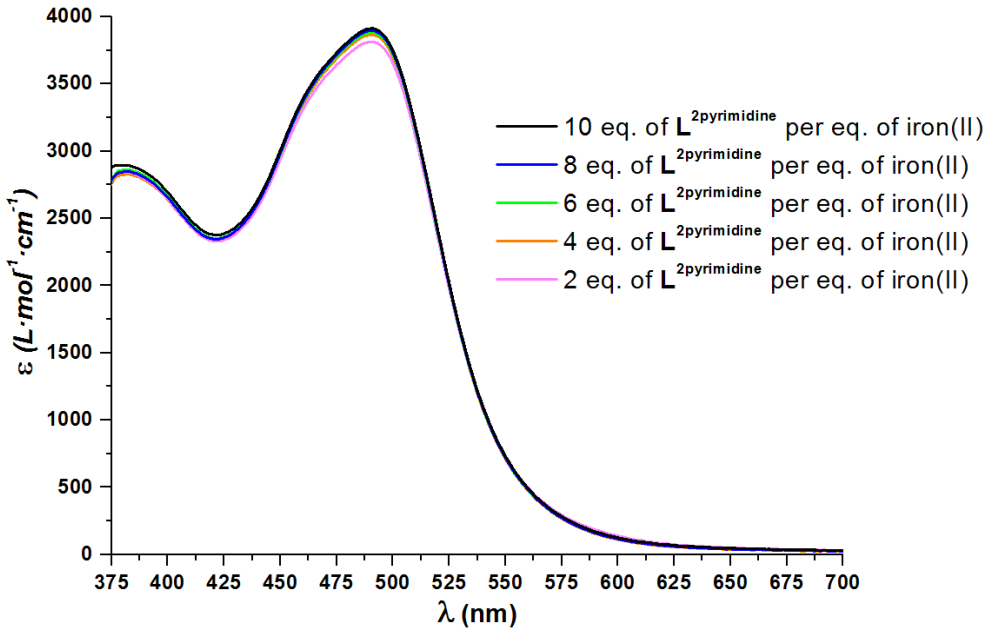

Figure S31. UV-Vis spectra of the speciation study of compound $[Fe^{II}(\mathbf{L^{2pyrimidine}})_2(NCBH_3)_2]$ in CH_3NO_2 using different $\mathbf{L^{2pyrimidine}}/Fe^{II}$ ratios.

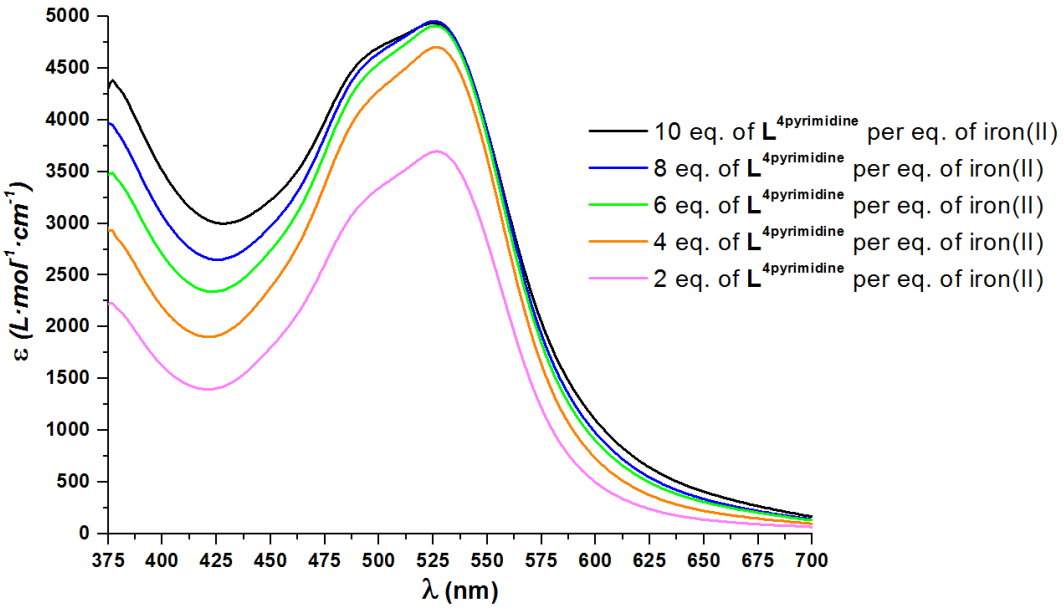

Figure S32. UV-Vis spectra of the speciation study of compound $[Fe^{II}(\mathbf{L}^{\mathbf{4pyrimidine}})_2(NCBH_3)_2]$ in CH_3NO_2 using different $\mathbf{L}^{\mathbf{2pyrimidine}}/Fe^{II}$ ratios.

S4.7. Comparison of UV-Vis spectra of $[Fe^{II}(L^{npyrimidine})_2(NCBH_3)_2]$ and $[Fe^{II}(L^{npyrimidine})_3](BF_4)_2$ complexes across solvents

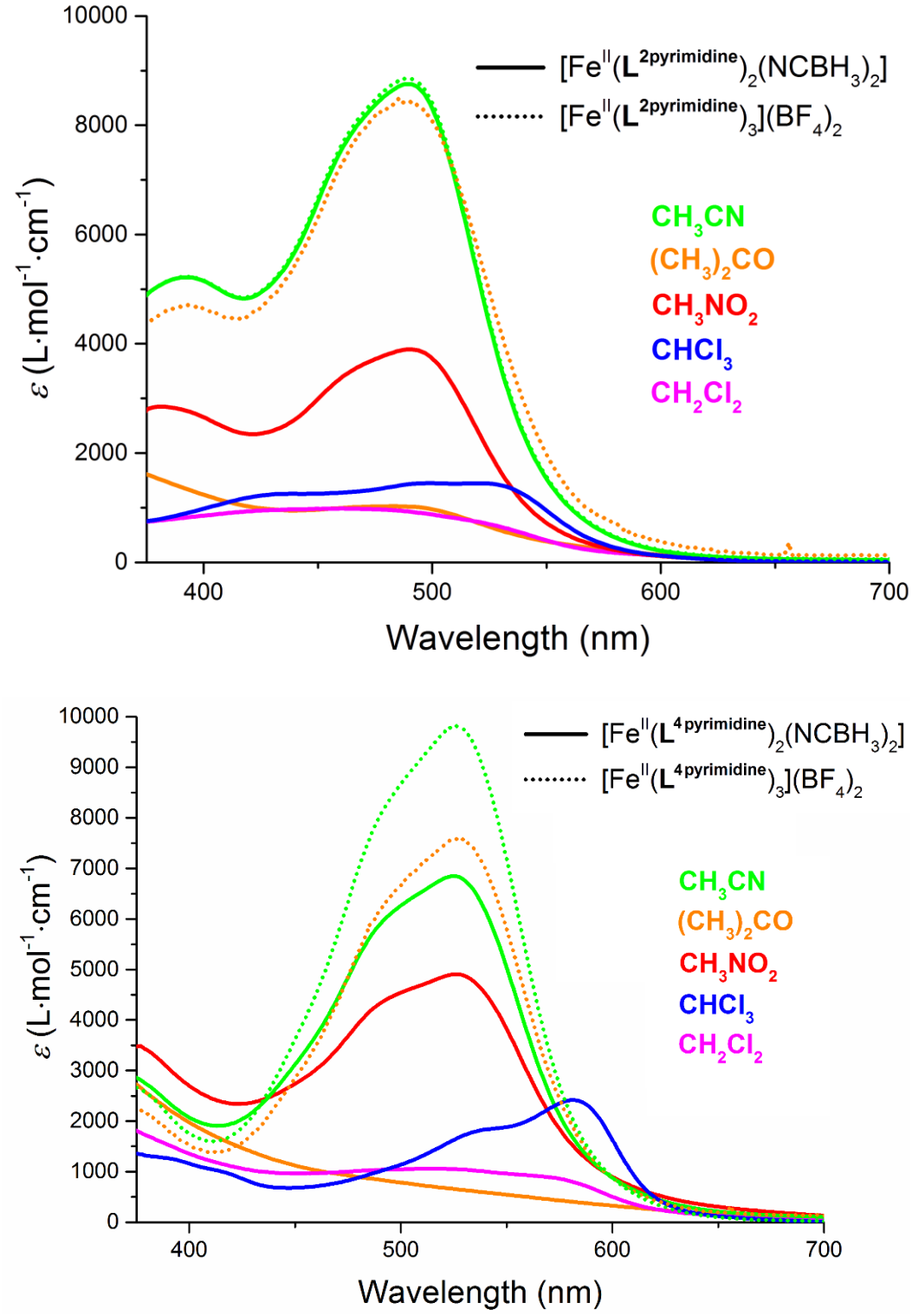

Figure S33. Overlays of the UV-Vis spectra of the $[Fe^{II}(L^{npyrimidine})_2(NCBH_3)_2]$ complexes in five different solvents (solid lines), compared with those of the related *tris*-ligand complexes, $[Fe^{II}(L^{npyrimidine})_3](BF_4)_2$,[11] in $(CH_3)_2CO$ and CH_3CN. Top: 2-pyrimidine complexes. Bottom: 4-pyrimidine complexes. All spectra run on solutions containing 6:1 $L^{npyrimidine}$ ligand per Fe.

S4.7. Comparison of UV-Vis spectra of $[Fe^{II}(L^{npyrimidine})_2(NCBH_3)_2]$ complexes in solution *versus* solid

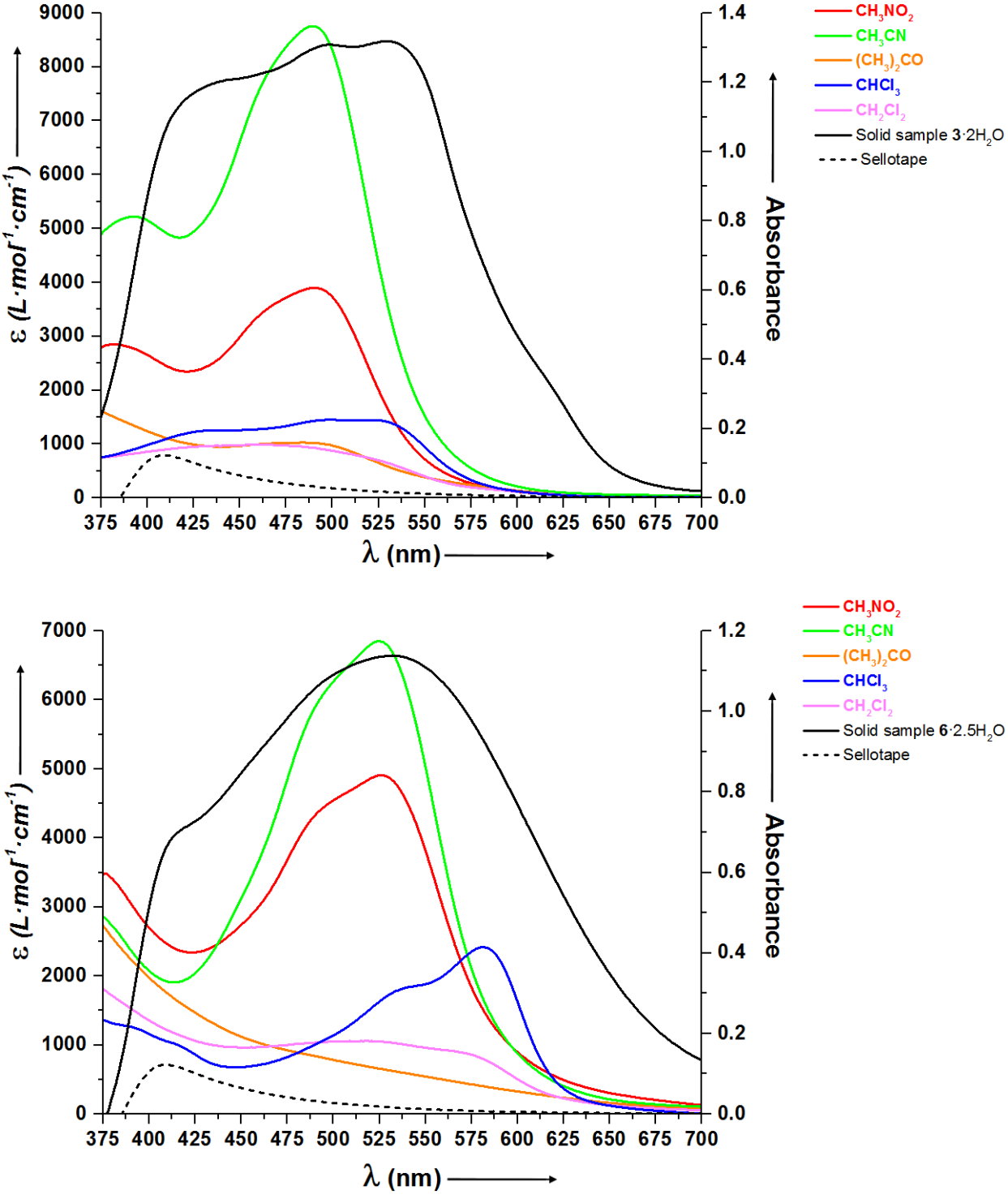

Figure S34. Overlays of the UV-Vis spectra of the $[Fe^{II}(\mathbf{L}^{npyrimidine})_2(NCBH_3)_2]$ complexes in five different solvents (colored solid lines; left axis), compared with that of the solid samples of complexes $[Fe^{II}(\mathbf{L}^{2pyrimidine})_2(NCBH_3)_2]\cdot 2H_2O$ (**3**·2H$_2$O, black solid line; right axis) and $[Fe^{II}(\mathbf{L}^{4pyrimidine})_2(NCBH_3)_2]\cdot 2.5H_2O$ (**3**·2H$_2$O, black solid line). Top: 2-pyrimidine complexes. Bottom: 4-pyrimidine complexes. All spectra run on solutions containing 6:1 $\mathbf{L}^{npyrimidine}$ ligand per Fe. Note that the double-sided Sellotape used to hold the solid samples is shown as a black dashed line.

S4.7. Tabulated data from the UV-Vis speciation study of $[Fe^{II}(L^{npyrimidine})_2(NCBH_3)_2]$ complexes

Table S9. Summary of observed bands in the UV-Vis bands for: (a) $CHCl_3$ solution of ligands $\mathbf{L^{2pyrimidine}}$ and $\mathbf{L^{4pyrimidine}}$, (b) complexes $[Fe^{II}(\mathbf{L^{2pyrimidine}})_2(NCBH_3)_2]$ (**3**) and $[Fe^{II}(\mathbf{L^{4pyrimidine}})_2(NCBH_3)_2]$ (**6**) measured in five different solvents, i.e. CH_2Cl_2, $CHCl_3$, $(CH_3)_2CO$, CH_3CN and CH_3NO_2, and (c) solid samples of complexes $[Fe^{II}(\mathbf{L^{2pyrimidine}})_2(NCBH_3)_2]\cdot 2H_2O$ (**3**·$2H_2O$) and $[Fe^{II}(\mathbf{L^{4pyrimidine}})_2(NCBH_3)_2]\cdot 2H_2O$ (**6**·$2.5H_2O$). Note that for the complexes the λ_{max} and molar extinction coefficients (ε) provided are for the spectra of solutions prepared using a 6:1 ratio of $\mathbf{L^{npyrimidine}}$ per iron(II). Also included is the wavelength maximum and associated absorbance value for the double-sided Sellotape used to hold the solid samples in place (Figure S34, black dashed line). Note that all spectra were collected at room temperature (approx. 293 K).

Phase	Compound	Solvent	λ_{max} / cm^{-1} (ε / $L{\cdot}mol^{-1}{\cdot}cm^{-1}$ or *Absorbance*)
Solution	Ligand $\mathbf{L^{2pyrimidine}}$	$CHCl_3$	268 (16396)
	Ligand $\mathbf{L^{4pyrimidine}}$	$CHCl_3$	284 (15523)
	$[Fe^{II}(\mathbf{L^{2pyrimidine}})_2(NCBH_3)_2]$ (**3**)	CH_2Cl_2	461 (986), 424 (946)
		$CHCl_3$	520 (1445), 498 (1449), 440 (1254)
		$(CH_3)_2CO$	482 (1026)
		CH_3CN	490 (8754), 465 (7870), 393 (5219)
		CH_3NO_2	491 (3885), 465 (3500)
	$[Fe^{II}(\mathbf{L^{4pyrimidine}})_2(NCBH_3)_2]$ (**6**)	CH_2Cl_2	566 (911), 517 (1059)
		$CHCl_3$	582 (2408), 543 (1815), 410 (908), 388 (1092)
		$(CH_3)_2CO$	477 (915)
		CH_3CN	525 (6848), 494 (6062)
		CH_3NO_2	526 (4908), 496 (4469)
Solid	$[Fe^{II}(\mathbf{L^{2pyrimidine}})_2(NCBH_3)_2]\cdot 2H_2O$ (**3**·$2H_2O$)	-	528 (*1.319*), 498 (*1.308*), 435 (*1.196*)
	$[Fe^{II}(\mathbf{L^{4pyrimidine}})_2(NCBH_3)_2]\cdot 2H_2O$ (**6**·$2.5H_2O$)	-	579 (*0.947*), 532 (*1.138*), 496 (*1.079*)
	Double-sided Sellotape	-	408 (*0.123*)

S5. Solution-phase spin crossover data of $[Fe^{II}(L^{npyrimidine})_2(NCBH_3)_2]$ complexes

S5.1. VT Evans' Method ^{1}H NMR measurements

The methodology to calculate $\chi_M T$ from Evans ^{1}H NMR method[12-14] has been previously described.[12-13, 15]

The population of HS species in solution, which can be expressed as $\chi_M T$, is directly dependent to temperature. Therefore, when HS and the LS states are in thermal equilibrium, or in other words: $T_{1/2}$, the observed temperature dependence can be reproduced by equation (1):[13, 16]

$$\chi_M T(T) = \frac{\chi_M T(\max)}{1+e^{\left(\frac{-\Delta H}{RT}+\frac{\Delta S}{R}\right)}} \quad (1)$$

Note that $\chi_M T(T)$ is $\chi_M T$ measured at an specific temperature T, $\chi_M T_{(max)}$ is the constant maximum $\chi_M T$ value equals to 3.5 emu·K·mol^{-1}, R is a constant (8.314472 J·mol^{-1}·K^{-1}), and ΔH and ΔS are the thermodynamic enthalpy and entropy values associated with the spin transition. The chosen maximum $\chi_M T$ falls within the expected literature range for iron(II) complexes.[16-18] The $T_{1/2}$ value can be calculated by dividing $\Delta H/\Delta S$.

Note that Evans method has a relative error of 5%,[19] therefore significant errors associated with the data fitting herein are expected. The derived parameters are reported in Table 2. The modeling of the each dataset, as a gradual and complete SCO, were carried out with *OriginPro version 9.1.0 from OriginLab Corporation* using the regular solution model [equation (1)][14, 20-21] with good fits.

S5.2. Tabulated solution-phase magnetic susceptibility data of $[Fe^{II}(L^{npyrimidine})_2(NCBH_3)_2]$ complexes

Table S10. Molar magnetic susceptibility ($\chi_M T$ in $cm^3 \cdot K \cdot mol^{-1}$) and HS molar fraction (γ_{HS}, within brackets) values calculated from Evans ^1H NMR data[12-13, 15] at different temperatures for complexes $[Fe^{II}(\mathbf{L^{2pyrimidine}})_2(NCBH_3)_2]$ (**3**) and $[Fe^{II}(\mathbf{L^{4pyrimidine}})_2(NCBH_3)_2]$ (**6**) in CD_2Cl_2, $CDCl_3$ (note these data are taken from ref. [15]) and $(CD_3)_2CO$ solution. Note that all concentrations are based on moles of $[Fe^{II}(pyridine)_4(NCBH_3)_2]$,[22] and each solution has used a $\mathbf{L^{npyrimidine}}$/Fe ratio of 6:1 (see section S4). Evans method has a relative error of 5%,[16] therefore significant errors associated with the data fitting are expected.

Temp. (K)	**3**	**6**	**3**[a]	**6**[a]	**3**	**6**
Deuterated solvent	CD_2Cl_2	CD_2Cl_2	$CDCl_3$	$CDCl_3$	$(CD_3)_2CO$	$(CD_3)_2CO$
Conc. (x 10^{-3} M)	5.00	5.03	4.58	4.75	2.50[b]	5.01
313	-	-	2.965 (0.847)	3.310 (0.946)	-	-
308	-	-	2.900 (0.829)	3.306 (0.944)	1.726 (0.493)	2.213 (0.632)
303	-	-	2.840 (0.811)	3.252 (0.929)	1.588 (0.454)	2.011 (0.575)
298	-	-	2.758 (0.788)	3.207 (0.916)	1.418 (0.405)	1.881 (0.538)
293	3.208 (0.917)	3.413 (0.975)	2.655 (0.759)	3.135 (0.896)	1.277 (0.365)	1.779 (0.508)
288	3.134 (0.895)	3.392 (0.969)	2.556 (0.730)	3.078 (0.879)	1.170 (0.334)	1.671 (0.478)
283	3.028 (0.865)	3.359 (0.960)	2.430 (0.694)	3.014 (0.861)	1.078 (0.308)	1.550 (0.443)
278	2.931 (0.837)	3.318 (0.948)	2.299 (0.657)	2.937 (0.840)	0.998 (0.285)	1.418 (0.405)
273	2.807 (0.802)	3.280 (0.937)	2.148 (0.614)	2.854 (0.815)	0.888 (0.254)	1.290 (0.369)
268	2.656 (0.759)	3.213 (0.918)	1.977 (0.565)	2.787 (0.796)	0.797 (0.228)	1.151 (0.329)
263	2.487 (0.711)	3.163 (0.904)	1.769 (0.505)	2.686 (0.767)	0.683 (0.195)	1.019 (0.291)
258	2.312 (0.661)	3.094 (0.884)	1.573 (0.449)	2.579 (0.737)	0.622 (0.178)	0.900 (0.257)
253	2.108 (0.602)	3.018 (0.862)	1.364 (0.390)	2.432 (0.695)	0.534 (0.153)	0.780 (0.223)
248	1.814 (0.518)	2.951 (0.8432)	1.254 (0.358)	2.316 (0.662)	0.466 (0.133)	0.649 (0.185)
243	1.445 (0.413)	2.861 (0.817)	1.088 (0.311)	2.231 (0.637)	0.417 (0.119)	0.575 (0.164)

[a] Note these data are taken from ref. [10]; and are shown here simply to facilitate comparison with the different tabulated values.

[b] Concentration is lower due to lower solubility.

Table S11. Molar magnetic susceptibility ($\chi_M T$ in $cm^3 \cdot K \cdot mol^{-1}$) and HS molar fraction (γ_{HS}, within brackets) values calculated from Evans ^1H NMR data[12-13, 15] at different temperatures for complexes $[Fe^{II}(\mathbf{L^{2pyrimidine}})_2(NCBH_3)_2]$ (**3**) and $[Fe^{II}(\mathbf{L^{4pyrimidine}})_2(NCBH_3)_2]$ (**6**) in CD_3CN and CD_3NO_2 solution. Note that all concentrations are based on moles of $[Fe^{II}(pyridine)_4(NCBH_3)_2]$,[22] and each solution has used a $\mathbf{L^{npyrimidine}}$/Fe ratio of 6:1 (see section S4). Evans method has a relative error of 5%,[16] therefore significant errors associated with the data fitting are expected.

Temp. (K)	**3**	**6**	**3**	**6**
Deuterated solvent	CD_3CN	CD_3CN	CD_3NO_2	CD_3NO_2
Conc. (x 10^{-3} M)	3.97[a]	3.97[a]	5.00	5.03
353	-	-	0.721 (0.206)	1.641 (0.469)
348	-	-	0.637 (0.182)	1.517 (0.433)
343	-	-	0.584 (0.167)	1.371 (0.392)
338	-	-	0.479 (0.137)	1.282 (0.366)
333	0.935 (0.267)	1.938 (0.554)	0.409 (0.117)	1.239 (0.354)
328	0.778 (0.222)	1.758 (0.502)	0.368 (0.105)	1.110 (0.317)
323	0.580 (0.166)	1.489 (0.426)	0.281 (0.080)	0.993 (0.284)
318	0.462 (0.132)	1.328 (0.379)	0.199 (0.057)	0.908 (0.259)
313	0.372 (0.106)	1.214 (0.347)	0.175 (0.050)	0.831 (0.237)
308	0.281 (0.080)	1.078 (0.308)	0.173 (0.050)	0.760 (0.217)
303	0.196 (0.056)	1.006 (0.288)	0.121 (0.034)	0.702 (0.201)
298	0.185 (0.053)	0.954 (0.273)	0.101 (0.029)	0.643 (0.184)
293	0.094 (0.027)	0.865 (0.247)	0.073 (0.021)	0.591 (0.169)
288	[b]	0.773 (0.221)	0.051 (0.014)	0.527 (0.151)
283	[b]	0.676 (0.193)	0.041 (0.012)	0.479 (0.137)
278	[b]	0.620 (0.177)	[b]	0.430 (0.123)
273	[b]	0.553 (0.158)	[b]	0.404 (0.116)
268	[b]	0.515 (0.147)	[b]	0.375 (0.107)
263	[b]	0.428 (0.122)	[b]	0.325 (0.093)
258	[b]	0.417 (0.119)	[b]	0.281 (0.080)
253	[b]	0.336 (0.096)	[b]	0.249 (0.071)
248	[b]	0.259 (0.074)	[b]	0.226 (0.065)
243	[b]	-	-	-

[a] Concentration is lower due to lower solubility.

S5.3 VT ^{1}H NMR spectra of $[Fe^{II}(L^{npyrimidine})_3](BF_4)_2$ complexes

S5.3.1. VT ^{1}H NMR spectra of $[Fe^{II}(L^{npyrimidine})_2(NCBH_3)_2]$ complexes in $CDCl_3$ solution

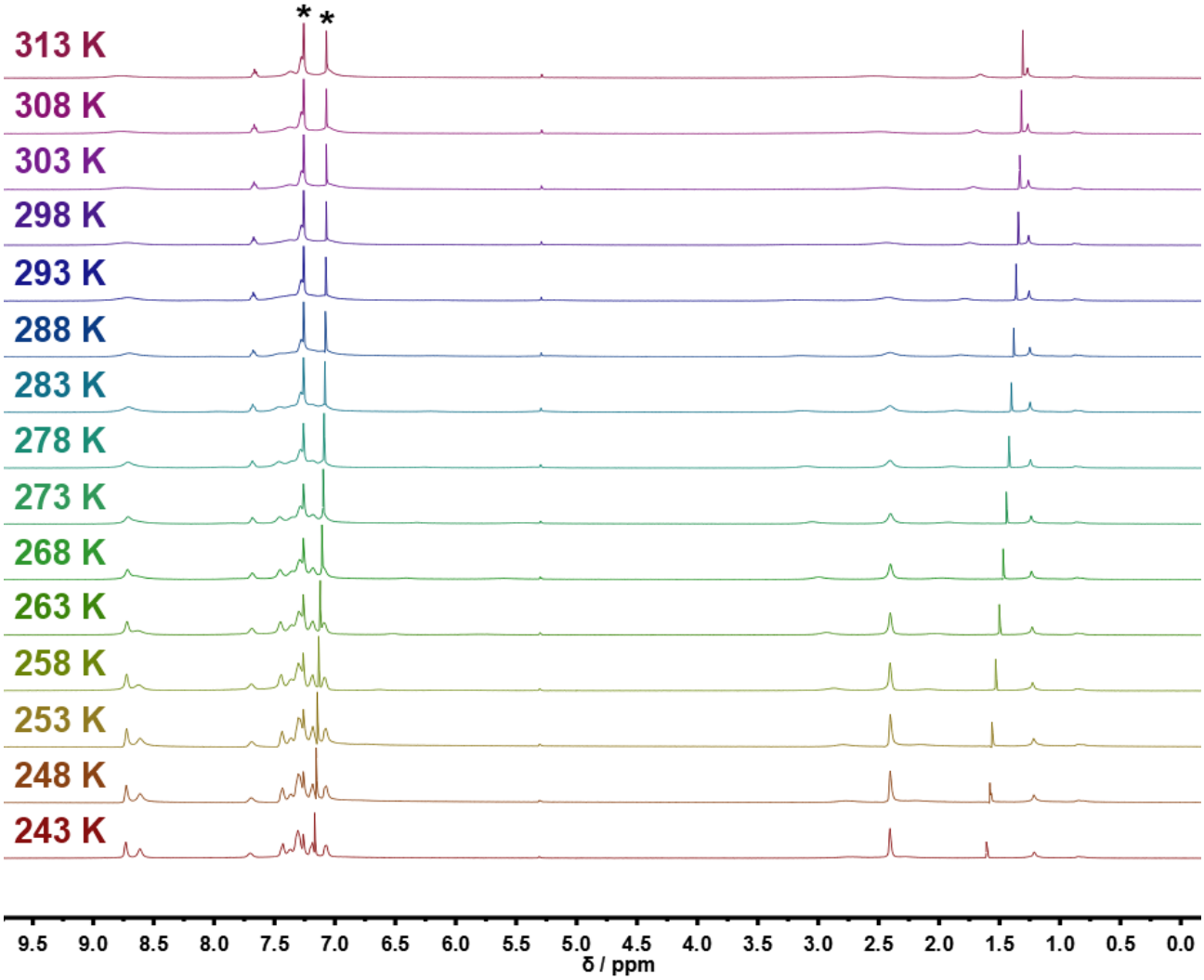

Figure S35. Stacked spectra, obtained by the Evans ^{1}H NMR method, from 313 to 243 K for complex $[Fe^{II}(\mathbf{L^{2pyrimidine}})_2(NCBH_3)_2]$ (**3**) in $CDCl_3$. Note that the solution was prepared using 6 eq. of $\mathbf{L^{2pyrimidine}}$ ligand per eq. of iron(II).

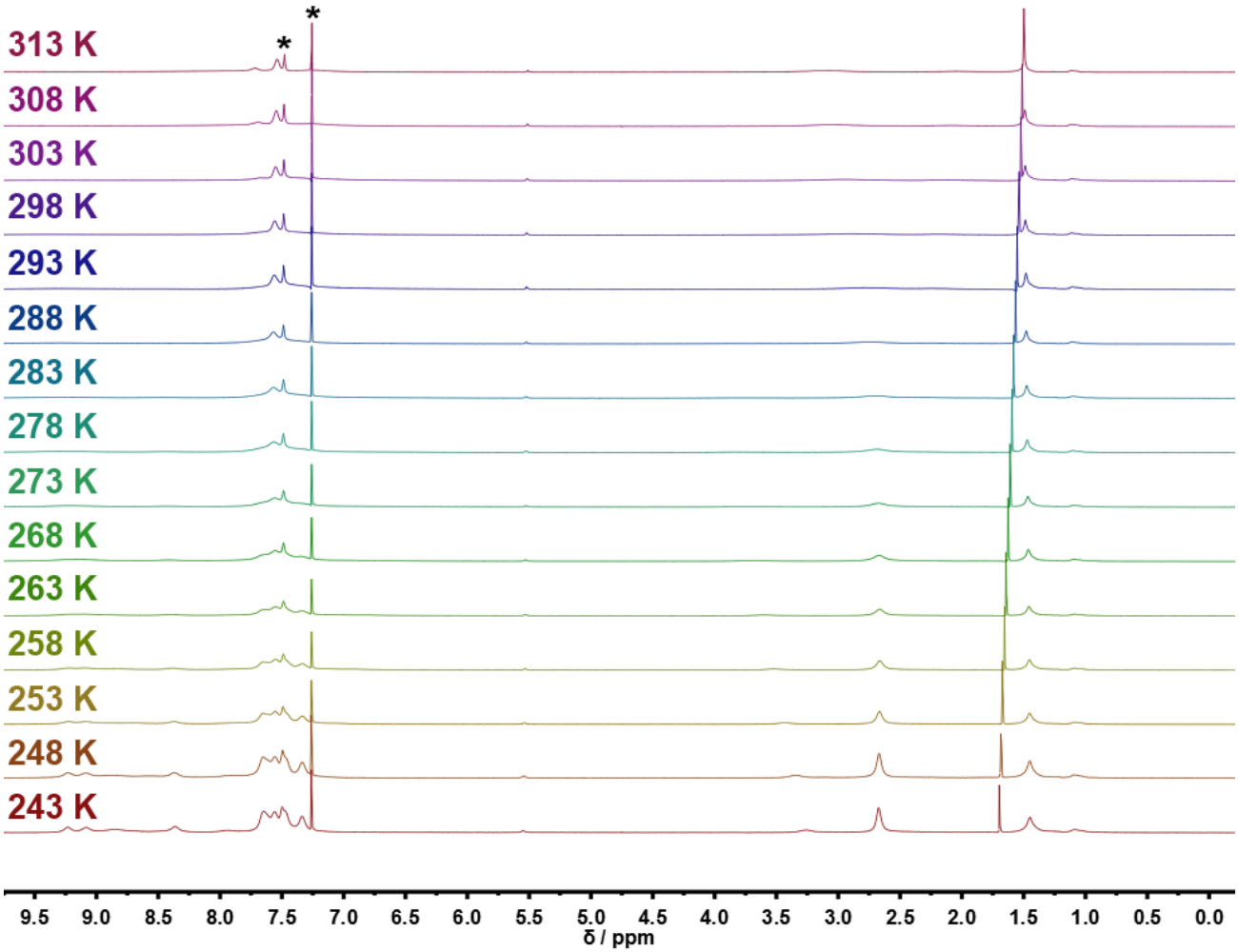

Figure S36. Stacked spectra, obtained by the Evans ^{1}H NMR method, from 313 to 243 K for complex $[Fe^{II}(\mathbf{L}^{4pyrimidine})_2(NCBH_3)_2]$ (**6**) in $CDCl_3$. Note that the solution was prepared using 6 eq. of $\mathbf{L}^{4pyrimidine}$ ligand per eq. of iron(II).

S5.3.2. VT ^{1}H NMR spectra of [Fe($L^{npyrimidine}$)$_2$($NCBH_3$)$_2$] complexes in CD_2Cl_2 solution

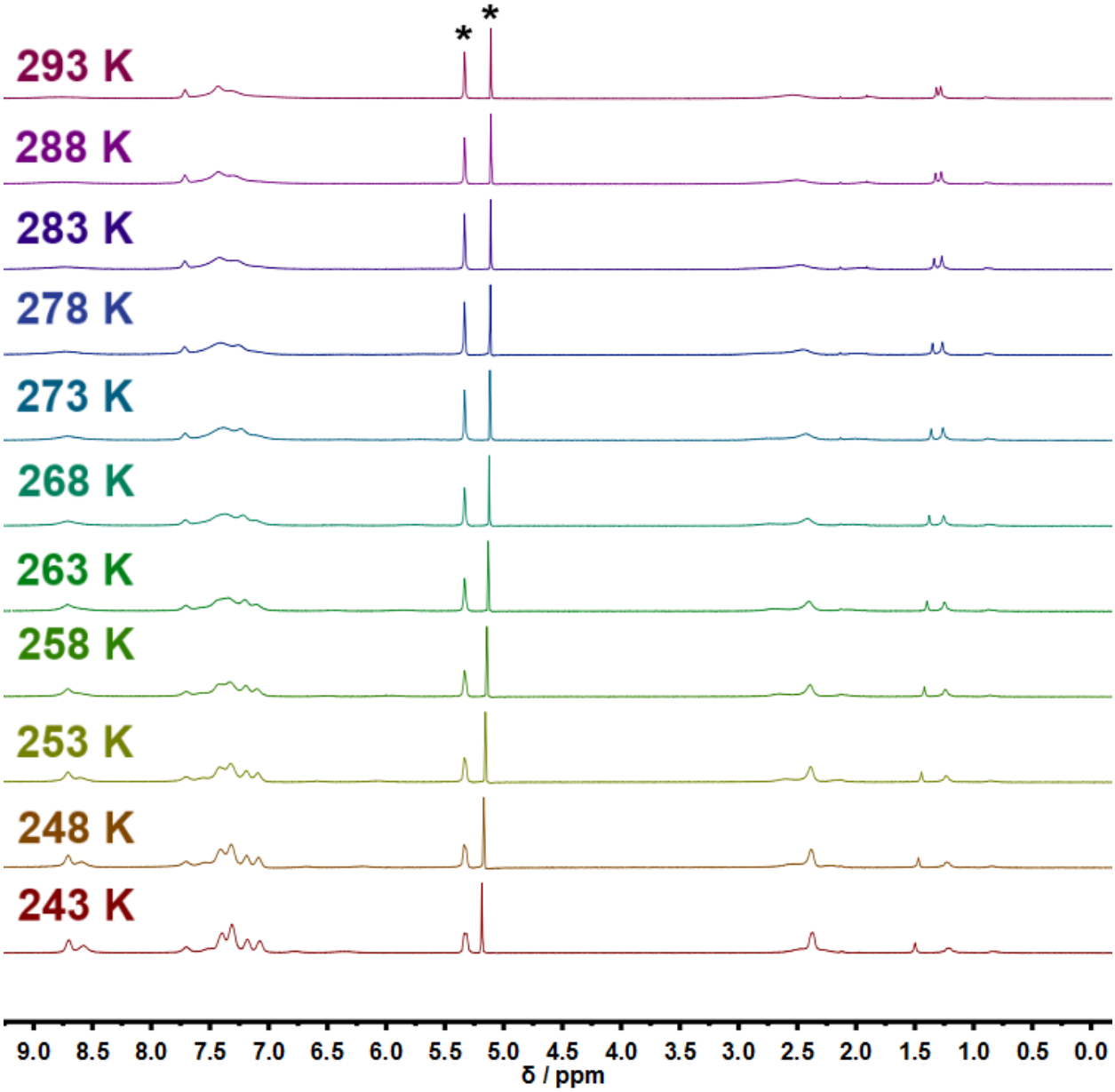

Figure S37. Stacked spectra, obtained by the Evans ^{1}H NMR method, from 293 to 243 K for complex [Fe^{II}(**$L^{2pyrimidine}$**)$_2$($NCBH_3$)$_2$] (**3**) in CD_2Cl_2. Note that the solution was prepared using 6 eq. of **$L^{2pyrimidine}$** ligand per eq. of iron(II).

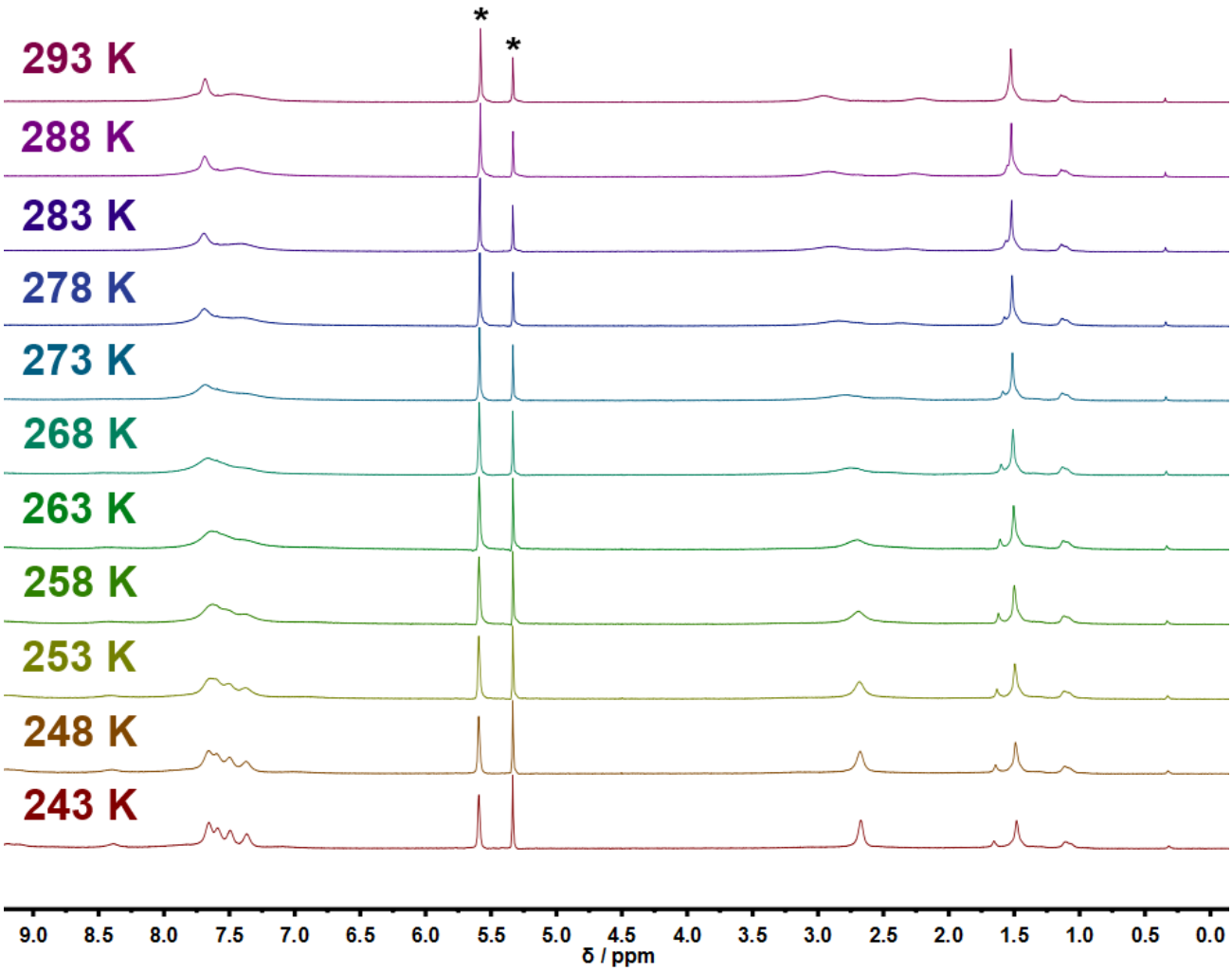

Figure S38. Stacked spectra, obtained by the Evans ^{1}H NMR method, from 293 to 243 K for complex $[Fe^{II}(\mathbf{L}^{4pyrimidine})_2(NCBH_3)_2]$ (**6**) in CD_2Cl_2. Note that the solution was prepared using 6 eq. of $\mathbf{L}^{4pyrimidine}$ ligand per eq. of iron(II).

S5.3.3. VT ^{1}H NMR spectra of $[Fe^{II}(L^{npyrimidine})_2(NCBH_3)_2]$ complexes in $(CD_3)_2CO$ solution

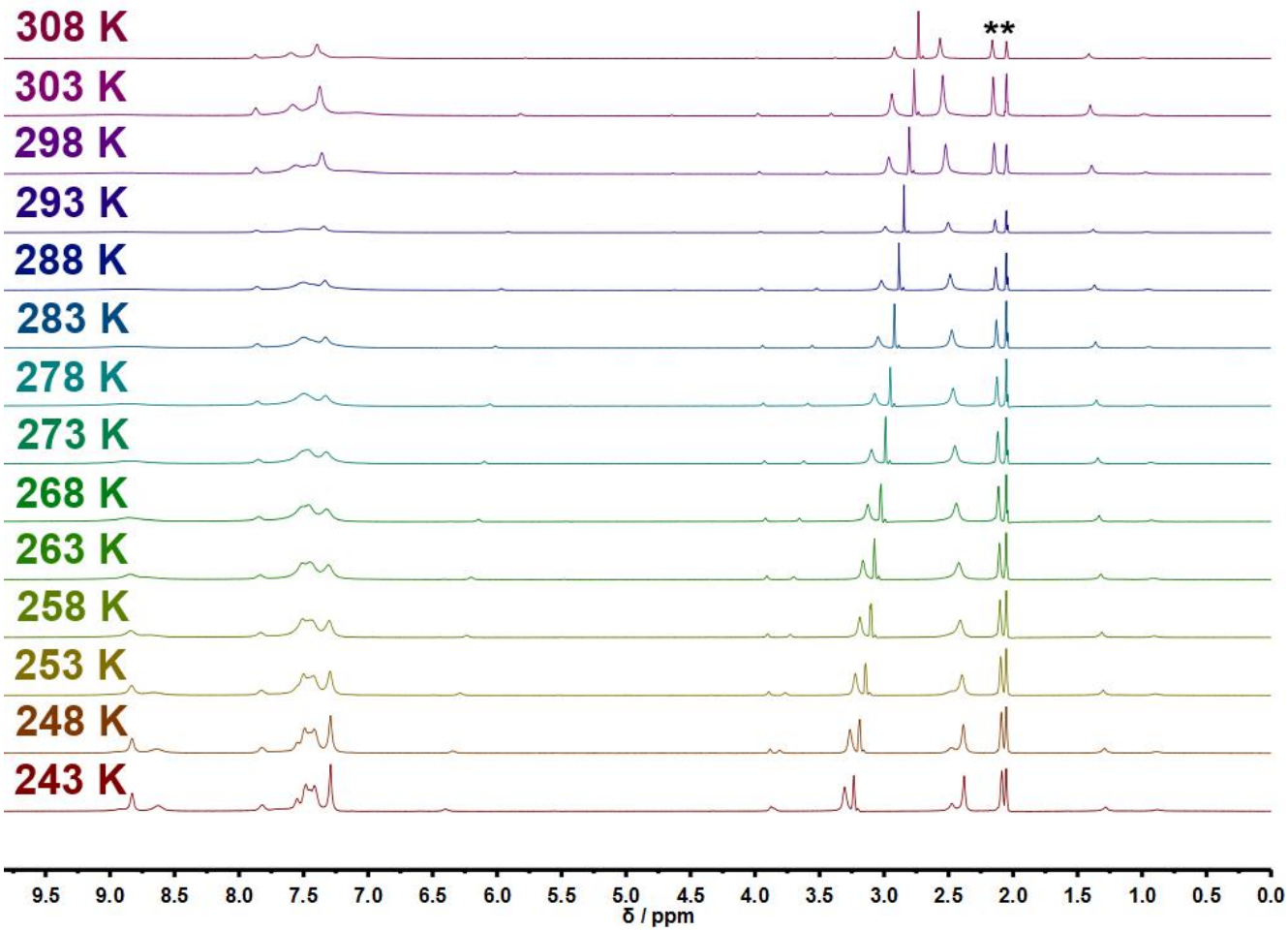

Figure S39. Stacked spectra, obtained by the Evans ^{1}H NMR method, from 308 to 243 K for complex $[Fe^{II}(\mathbf{L^{2pyrimidine}})_2(NCBH_3)_2]$ (**3**) in $(CD_3)_2CO$. Note that the solution was prepared using 6 eq. of $\mathbf{L^{2pyrimidine}}$ ligand per eq. of iron(II).

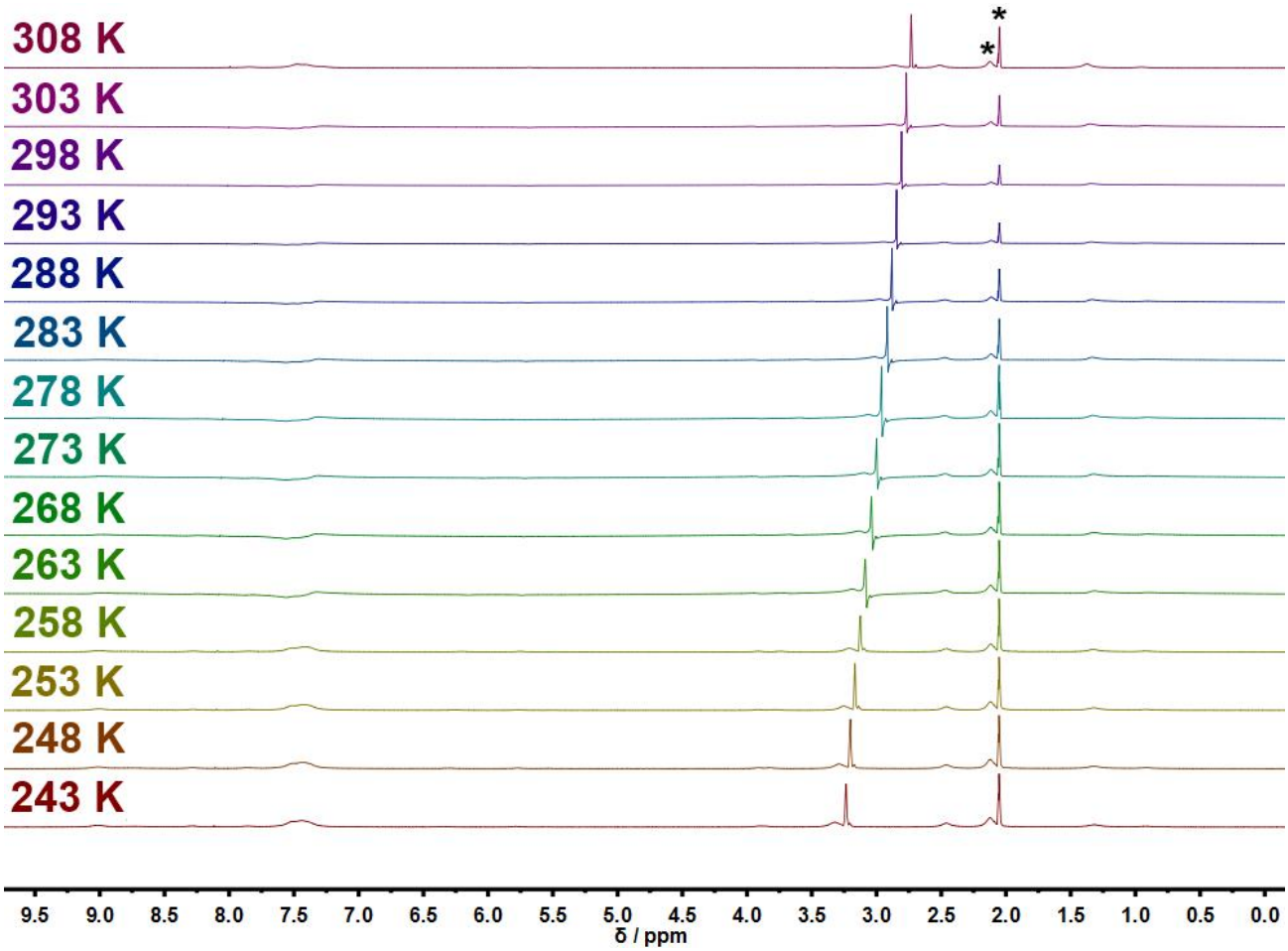

Figure S40. Stacked spectra, obtained by the Evans ^{1}H NMR method, from 308 to 243 K for complex $[Fe^{II}(\mathbf{L^{4pyrimidine}})_2(NCBH_3)_2]$ (**6**) in $(CD_3)_2CO$. Note that the solution was prepared using 6 eq. of $\mathbf{L^{4pyrimidine}}$ ligand per eq. of iron(II).

S5.3.4. VT ^{1}H NMR spectra of $[Fe^{II}(L^{npyrimidine})_2(NCBH_3)_2]$ complexes in CD_3CN solution

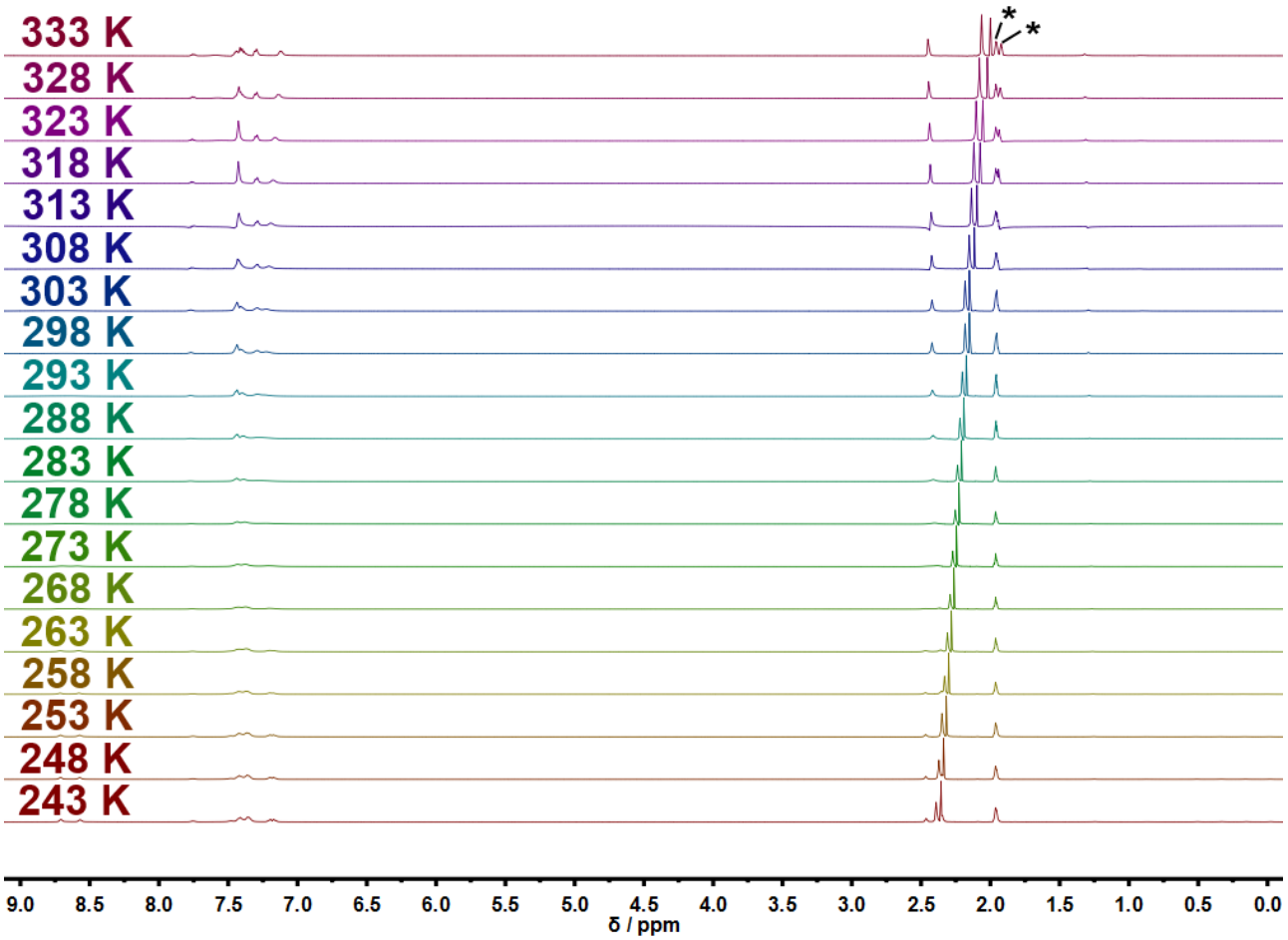

Figure S41. Stacked spectra, obtained by the Evans ^{1}H NMR method, from 333 to 243 K for complex $[Fe^{II}(\mathbf{L^{2pyrimidine}})_2(NCBH_3)_2]$ (**3**) in CD_3CN. Note that the solution was prepared using 6 eq. of $\mathbf{L^{2pyrimidine}}$ ligand per eq. of iron(II).

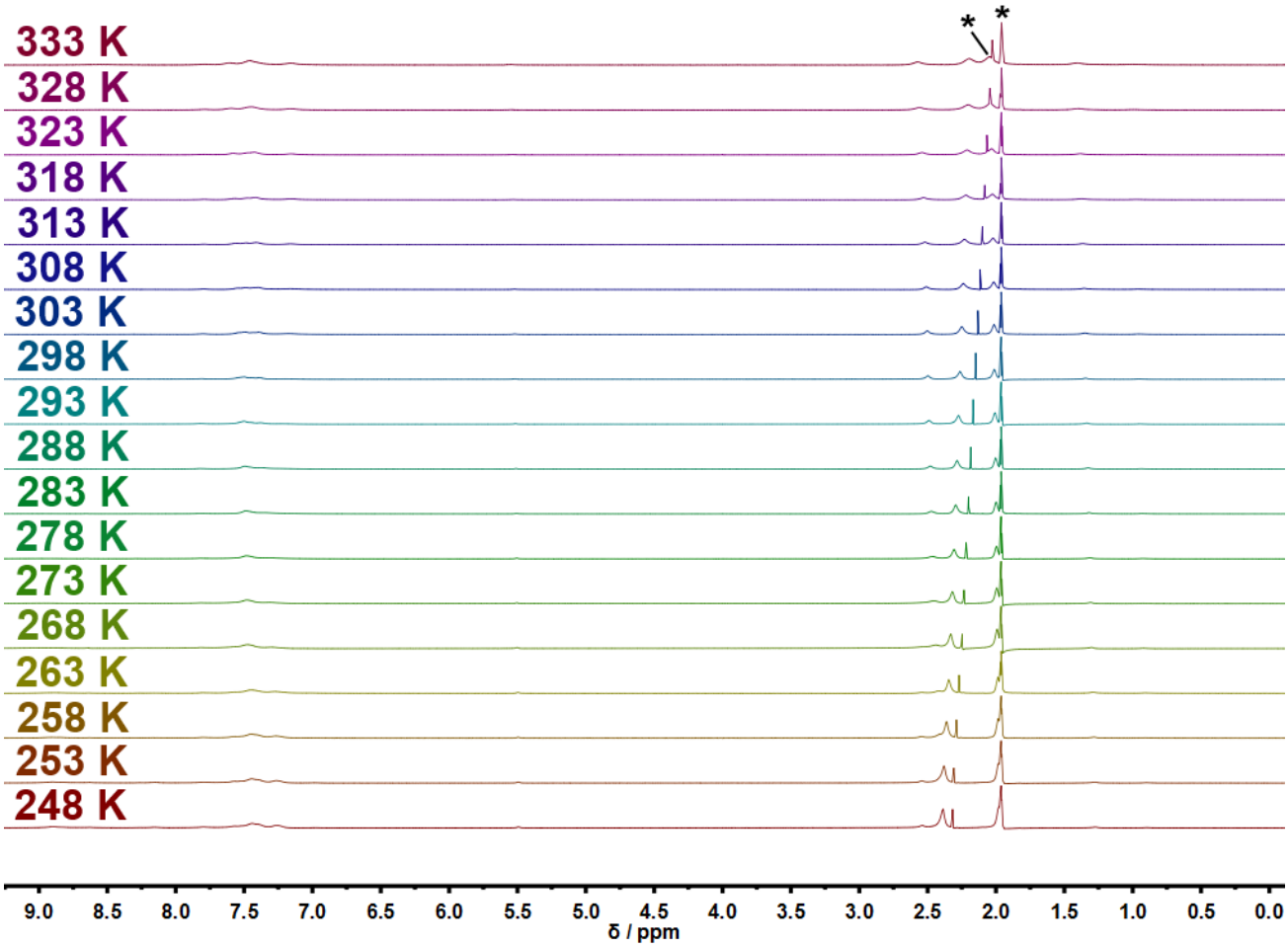

Figure S42. Stacked spectra, obtained by the Evans ^{1}H NMR method, from 333 to 248 K for complex $[Fe^{II}(\mathbf{L}^{\mathbf{4pyrimidine}})_2(NCBH_3)_2]$ (**6**) in CD_3CN. Note that the solution was prepared using 6 eq. of $\mathbf{L}^{\mathbf{4pyrimidine}}$ ligand per eq. of iron(II).

S5.3.5. VT ^{1}H NMR spectra of $[Fe^{II}(L^{npyrimidine})_2(NCBH_3)_2]$ complexes in CD_3NO_2 solution

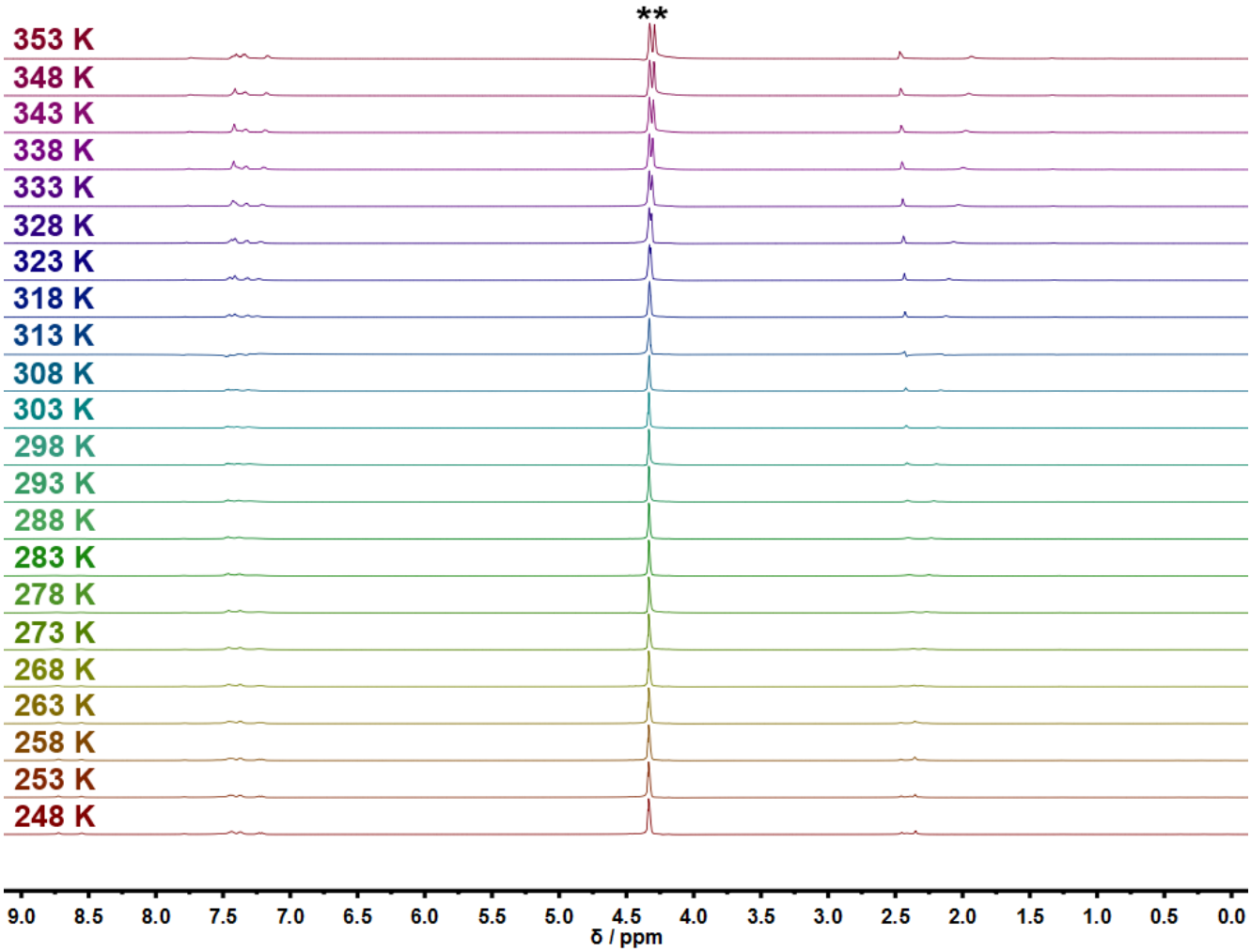

Figure S43. Stacked spectra, obtained by the Evans ^{1}H NMR method, from 353 to 248 K for complex $[Fe^{II}(\mathbf{L^{2pyrimidine}})_2(NCBH_3)_2]$ (**3**) in CD_3NO_2. Note that the solution was prepared using 6 eq. of $\mathbf{L^{2pyrimidine}}$ ligand per eq. of iron(II).

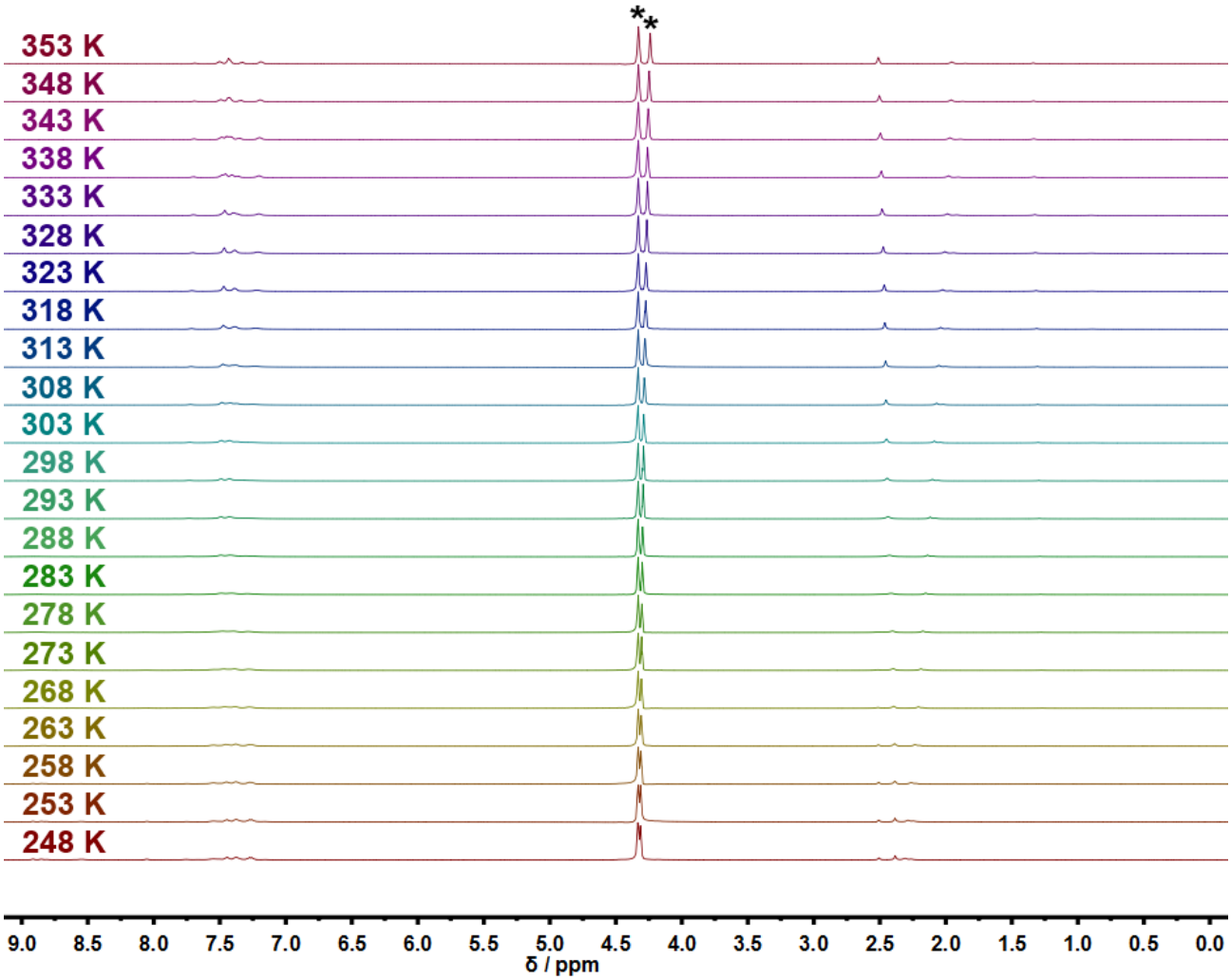

Figure S44. Stacked spectra, obtained by the Evans ^{1}H NMR method, from 333 to 248 K for complex $[Fe^{II}(\mathbf{L}^{\mathbf{4pyrimidine}})_2(NCBH_3)_2]$ (**6**) in CD_3NO_2. Note that the solution was prepared using 6 eq. of $\mathbf{L}^{\mathbf{4pyrimidine}}$ ligand per eq. of iron(II).

S5.4. Correlations between $T_{1/2}$ and different solvent parameters and physical properties

S5.4.1. Tabulated values of the different solvent parameters and physical properties

Table S12. Tabulated values of the solvent parameters: i.e. Reichardt's E_T^N parameter,[23] polarity index (P'),[24-25] basity,[26-27] and physical properties: Hildebrand's solvent solubility parameter (δ, $MPa^{1/2}$),[28] relative permittivity or dielectric constant (ε_r) and the dipole moment (μ, D) of the five solvents used in this study and the $T_{1/2}$ values (K) of complexes $[Fe^{II}(\mathbf{L^{2pyrimidine}})_2(NCBH_3)_2]$ (**3**) and $[Fe^{II}(\mathbf{L^{4pyrimidine}})_2(NCBH_3)_2]$ (**6**). Note that the solvent parameters and physical properties herein tabulated are those that showed the best correlations with $T_{1/2}$ (Figures 14 and S45-S50). If units are not stated, the parameters are dimensionless.

Solvent	P'[a]24-25	P'25	E_T^N[c]23	*Basity*[d]26-27	δ[e]28	ε_r[f]29	μ[g]	$T_{1/2}$ of **3**	$T_{1/2}$ of **6**
CH_2Cl_2	3.1	3.4	0.309	0.80	19.8	8.93	1.14	247	216
$CHCl_3$	4.1	4.3	0.259	0.73	19.0	4.81	1.15	262	232
$(CH_3)_2CO$	5.1	5.4	0.355	0.81	20.3	21.01	2.69	312	291
CH_3CN	5.8	6.2	0.460	0.86	24.3	36.64	3.44	353	334
CH_3NO_2	6.8	6.8	0.481	0.92	26.0	37.27	3.46	396	367

[a] The Polarity index (P')[24-25] is an empirical parameter that gives a relative measure of the degree of interaction of the solvent with various polar test solutes, i.e. ethanol, dioxane and nitromethane, which are used to gauge the strengths of solvent proton acceptor, proton donor and strong dipole interactions, respectively. The effects related to solute molecular size, solute/solvent dispersion interactions, and solute/solvent induction due to solvent polarizability are taken into account; thus, P' should reflect only the interaction properties of the solvent.[24, 30] Note that these tabulated P' values are used in Figure 14, and the P' values for CH_2Cl_2 (3.1), $CHCl_3$ (4.1), $(CH_3)_2CO$ (5.1) and CH_3CN (5.8) were reported by Ahuja in 2003[24], while the P' value for CH_3NO_2 (6.8) was reported by Schirmer in 1990[25].

[b] The tabulated P' values correspond to those reported by Schirmer in 1990[25], and represented against the $T_{1/2}$ values of compounds **3** and **6** in Figure S45.

[c] The Reichardt's E_T^N (Normalized *molar electronic Transition Energies*)[23] empirical parameter is a widely used scale of solvent polarity.

[d] Swain and co-workers' *Basity*[26-27] parameter represents the cation-solvating tendency, the hydrogen-bonding basicity and nucleophilic properties of a solvent.

[e] The Hildebrand's solvent solubility parameter (δ)[28] is used as an indicator of solvent polarity for regular solutions.

[f] ε_r corresponds to the relative permittivity or dielectric constant; [g] μ is to the dipole moment.

Table S13. Tabulated best R^2 values for the $T_{1/2}$ *values* of complexes [Fe^{II}(**$L^{2pyrimidine}$**)$_2$($NCBH_3$)$_2$] (**3**) and [Fe^{II}(**$L^{4pyrimidine}$**)$_2$($NCBH_3$)$_2$] (**6**) *versus* the solvent parameters and physical properties of the five solvents used in this study.

Compound	[Fe^{II}(**$L^{2pyrimidine}$**)$_2$($NCBH_3$)$_2$] (**3**)	[Fe^{II}(**$L^{4pyrimidine}$**)$_2$($NCBH_3$)$_2$] (**6**)
$T_{1/2}$ *vs* P'[a]	0.96	0.96
$T_{1/2}$ *vs* P'[b]	0.94	0.97
$T_{1/2}$ *vs* ε_r	0.89	0.92
$T_{1/2}$ *vs* μ	0.88	0.93
$T_{1/2}$ *vs* E_N^T	0.86	0.87
$T_{1/2}$ *vs* δ	0.86	0.83
$T_{1/2}$ *vs Basity*	0.74	0.71

[a] These R^2 values are shown in Figure 14 and discussed in the main manuscript. They were obtained from ref. [24-25] (see table caption above).

[b] These R^2 values were obtained from using the P' values (see Figure S45) reported by Schirmer in 1990[25].

Table S14. Tabulated values of the solvent parameters: *Acity*,[26-27] *α*,[26, 31] *β*,[26, 31] *π**, *SB*,[32] *SA*, *DN*[33-34] *and AN*[35] of the five solvents used in this study and the $T_{1/2}$ values of complexes $[Fe^{II}(\mathbf{L^{2pyrimidine}})_2(NCBH_3)_2]$ (**3**) and $[Fe^{II}(\mathbf{L^{4pyrimidine}})_2(NCBH_3)_2]$ (**6**). Note that the solvent parameters herein tabulated have shown poor or no correlation with $T_{1/2}$. If units are not stated, the parameters are dimensionless.

Solvent	*Acity*[a]26-27	*α*[b]26, 31	β[c]26, 31	*π**[d]26, 31	*SB*[e]32	*SA*[f]32	*DN*[g]33-34	*AN*[h]33-34	$T_{1/2}$ of **3**	$T_{1/2}$ of **6**
CH_2Cl_2	0.33	0.13	0.1	0.82	0.178	0.04	1.0	20.4	247	216
$CHCl_3$	0.42	0.1	0.2	0.58	0.071	0.047	4.0	23.1	262	232
$(CH_3)_2CO$	0.25	0.08	0.43	0.71	0.475	0	17.0	12.5	312	291
CH_3CN	0.37	0.19	0.4	0.75	0.286	0.044	14.1	18.9	353	334
CH_3NO_2	0.39	0.22	0.06	0.85	0.236	0.078	2.7	20.5	396	367

[a] The Swain and co-workers' *acity*[26-27] parameter represents the anion-solvating tendency, the hydrogen-bonding acidity and the electrophilic properties of a solvent.

[b] The Kamlet and Taft's α[26, 31] parameter describes solvents based on their hydrogen-bond donor acidities, i.e the ability of the solvent to donate a proton in a solvent-to-solute hydrogen bond; while

[c] the β[26, 31] parameter describes solvents based on their hydrogen-bond acceptor basicities which provides a measure of the solvent's ability to accept a proton (donate an electron pair) in a solute-to-solvent hydrogen bond.[31]

[d] The π*[26, 31] parameter is an index of solvent dipolarity/polarizability, which measures the ability of the solvent to stabilize a charge or a dipole by virtue of its dielectric effect.

[e] Catalan and co-workers' *Solvent Basicity (SB)*[32] parameter classifies the basicity of solvents based on their hydrogen-bond acceptor ability, whilst

[f] the *Solvent Acidity* (*SA*)[32] parameter describes the acidity of solvents based on their hydrogen-bond donating ability.

[g] The Gutmann's *Donor Number* (*DN*)[33-34] is an empirical parameter used to describe the donor strength of a given solvent.

[h] The Mayer and Gutmann' *Acceptor Number* (*AN*)[35] is an empirical parameter that measures the electrophilic properties of solvents.

S5.4.2. Linear fits of $T_{1/2}$ versus different solvent parameters and physical properties

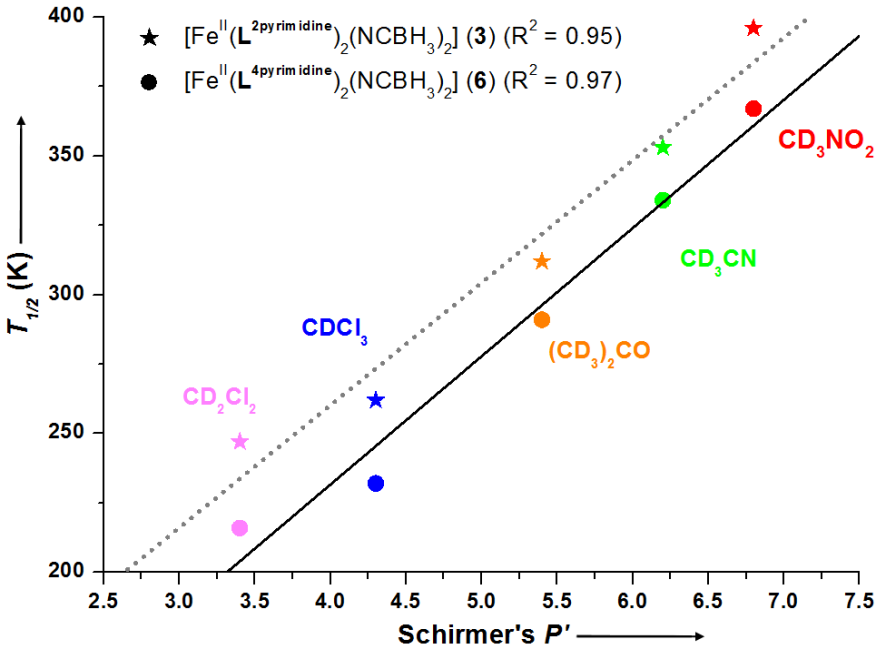

Figure S45. Plot of $T_{1/2}$ *versus* P' parameter reported by Schirmer in 1990[25] for complexes [Fe(**L**^{2pyrimidine})$_2$(NCBH$_3$)$_2$] (**3**) and [Fe(**L**^{4pyrimidine})$_2$(NCBH$_3$)$_2$] (**6**).

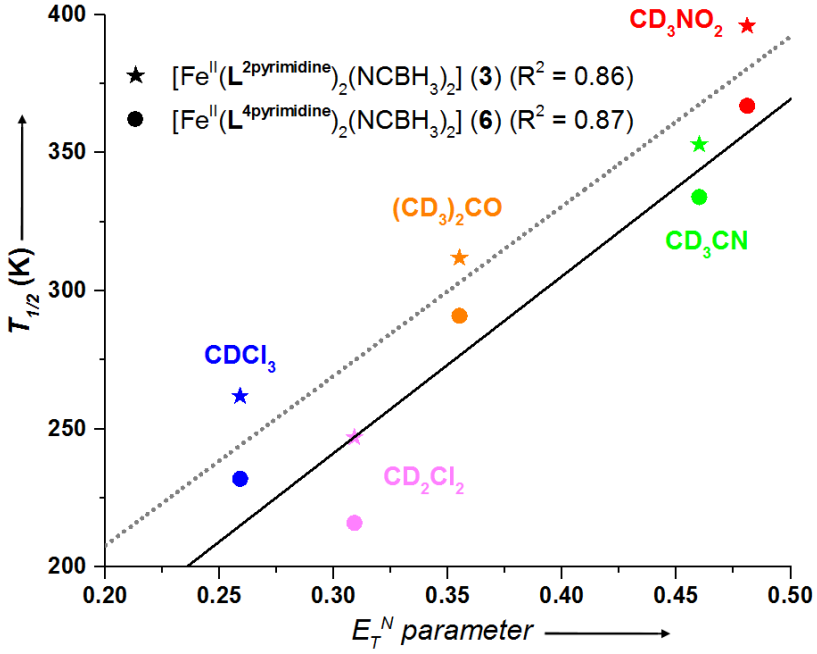

Figure S46. Plot of $T_{1/2}$ *versus* Reichardt's E_T^N parameter[23] for complexes [Fe(**L**^{2pyrimidine})$_2$(NCBH$_3$)$_2$] (**3**) and [Fe(**L**^{4pyrimidine})$_2$(NCBH$_3$)$_2$] (**6**).

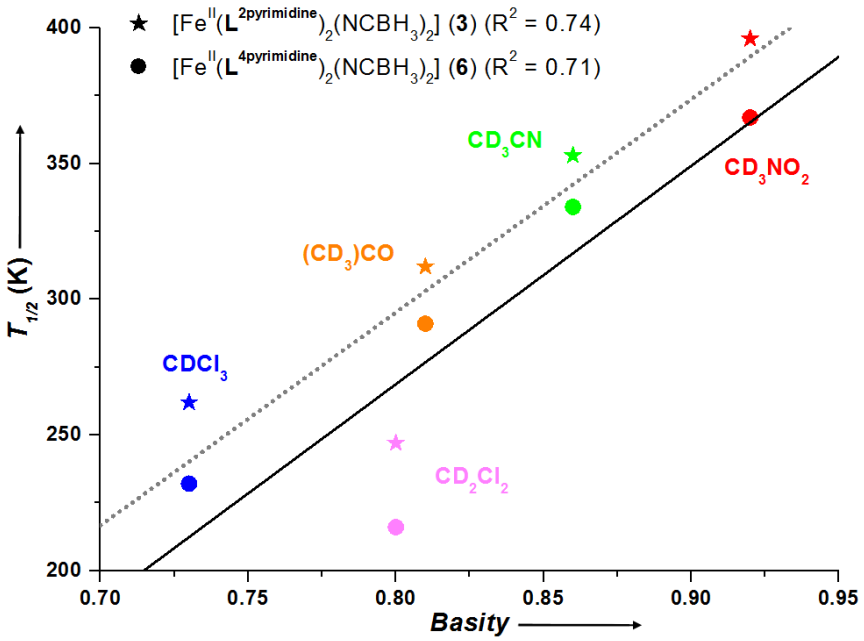

Figure S47. Plot of $T_{1/2}$ *versus* Swain and co-workers' *Basity* parameter[26-27] for complexes [Fe(**L**^{2pyrimidine})$_2$(NCBH$_3$)$_2$] (**3**, stars) and [Fe(**L**^{4pyrimidine})$_2$(NCBH$_3$)$_2$] (**6**, circles).

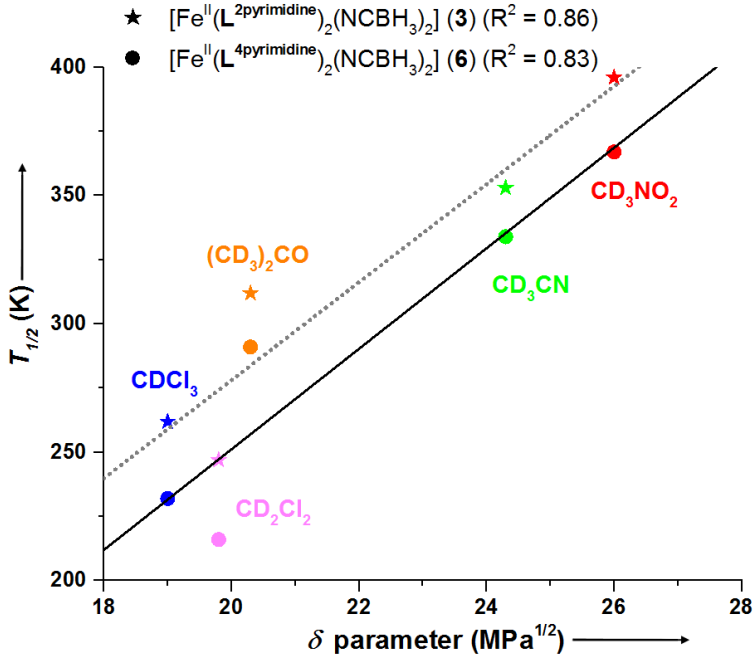

Figure S48. Plot of $T_{1/2}$ *versus* Hildebrand's solubility parameter (δ)[28] for complexes [Fe(**L**^{2pyrimidine})$_2$(NCBH$_3$)$_2$] (**3**, stars) and [Fe(**L**^{4pyrimidine})$_2$(NCBH$_3$)$_2$] (**6**, circles).

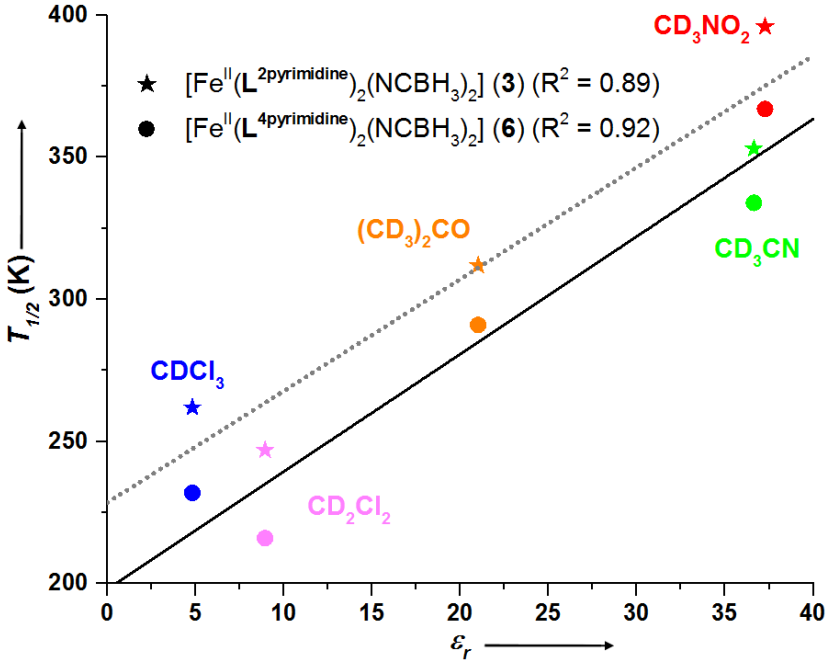

Figure S49. Plot of $T_{1/2}$ *versus* relative permittivity or dielectric constant (ε_r) for complexes [Fe(**L**^{2pyrimidine})$_2$(NCBH$_3$)$_2$] (**3**, stars) and [Fe(**L**^{4pyrimidine})$_2$(NCBH$_3$)$_2$] (**6**, circles).

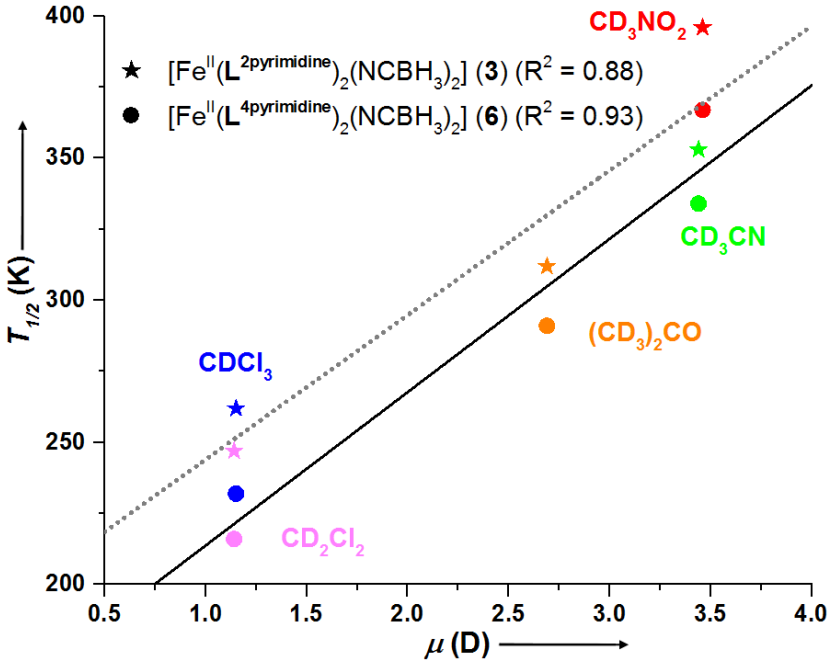

Figure S50. Plot of $T_{1/2}$ *versus* the dipole moment (μ) for complexes [Fe(**L**^{2pyrimidine})$_2$(NCBH$_3$)$_2$] (**3**) and [Fe(**L**^{4pyrimidine})$_2$(NCBH$_3$)$_2$] (**6**).

S5.5. Comparison of VT NMR data on $[Fe^{II}(L^{npyrimidine})_2(NCE)_2]$ and $[Fe^{II}(L^{npyrimidine})_3](BF_4)_2$ complexes

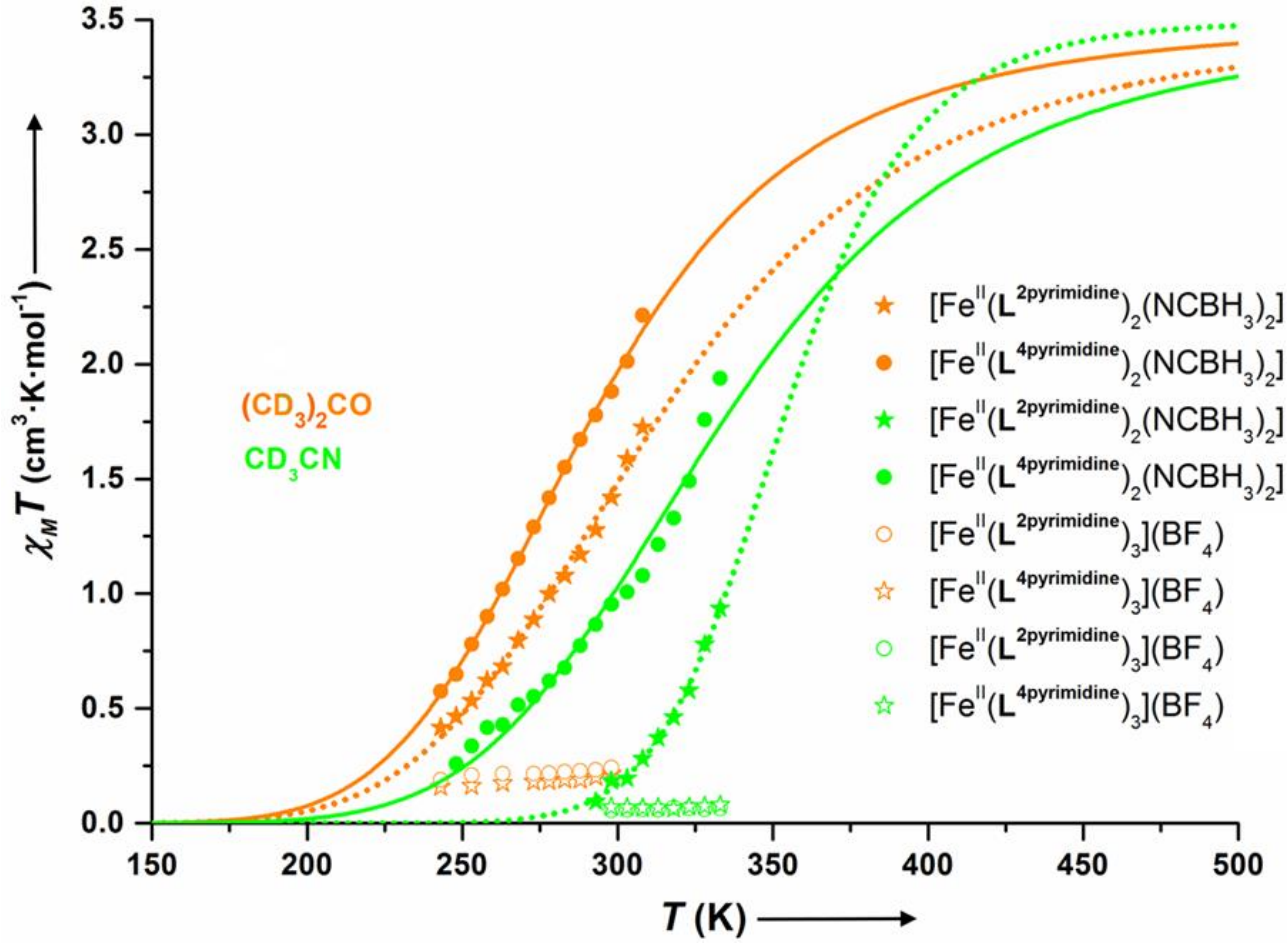

Figure S51**.** Solution-phase magnetic data presented as $\chi_M T$ *versus* T, in two different deuterated solvents, $(CD_3)_2CO$ (orange) and CD_3CN (green), for the pair of cyanoborohydride complexes reported in this paper, $[Fe^{II}(\mathbf{L^{2pyrimidine}})_2(NCBH_3)_2]$ (**3**, stars and dotted lines) and $[Fe^{II}(\mathbf{L^{4pyrimidine}})_2(NCBH_3)_2]$ (**6**, circles and solid lines), compared with that obtained for the pair of related *tris*-ligand complexes, $[Fe^{II}(\mathbf{L^{2pyrimidine}})_3](BF_4)_2$ (hollow stars) and $[Fe^{II}(\mathbf{L^{4pyrimidine}})_3](BF_4)_2$ (hollow circles).[11] Each solution was prepared using a 6:1 L:Fe ratio. The lines correspond to the best fit found for each compound using the regular solution model, equation (1).[14, 20-21]

S6. Conductivity measurements of $[Fe^{II}(L^{npyrimidine})_2(NCBH_3)_2]$ and $[Fe^{II}(L^{npyrimidine})_3](BF_4)_2$

All conductivity measurements were carried out at 25°C using dry solvents. The concentration of all solutions was $1{\cdot}10^{-3}$ M. The specific conductivities of acetonitrile and acetone at 25°C were $8{\cdot}10^{-7}$ S·cm^{-1} and $4{\cdot}10^{-7}$ S·cm^{-1}, respectively. Literature molar conductivity ranges for electrolyte solutions ($1{\cdot}10^{-3}$ M at 25°C with a 1:1 or 2:1 ion type) in each of these solvents follow:[36]

Acetone: 1:1 ion type 100-140 S·cm^2·mol^{-1} 2:1 ion type 160-200 S·cm^2·mol^{-1}

Acetonitrile: 1:1 ion type 120-160 S·cm^2·mol^{-1} 2:1 ion type 220-300 S·cm^2·mol^{-1}

Table S15. Molar conductivity values obtained for ligands $\mathbf{L^{2pyrimidine}}$ and $\mathbf{L^{4pyrimidine}}$, the iron(II) reagents $[Fe(pyridine)_2(NCBH_3)_2]$ and $[Fe(H_2O)_3](BF_4)_2$, the pair of cyanoborohydride complexes, $[Fe(\mathbf{L^{npyridimidine}})_2(NCBH_3)_2]$, using a $\mathbf{L^{npyrimidine}}$:Fe ratio of 2:1 or 6:1, are compared with those obtained for the related pair of *tris*-ligand complexes, $[Fe(\mathbf{L^{npyridimidine}})_3](BF_4)_2$,[11] using a $\mathbf{L^{npyrimidine}}$:Fe ratio of 3:1 or 6:1.

Solvent	Compound	Ratio of $\mathbf{L^{npyrimidine}}$:Fe eq.	Molar conductivity (S·cm^2·mol^{-1})
acetonitrile	$\mathbf{L^{2pyridimidine}}$	-	2
	$\mathbf{L^{4pyridimidine}}$	-	2
	$[Fe(pyridine)_2(NCBH_3)_2]$	-	41
	$[Fe(H_2O)_3](BF_4)_2$	-	286
	$[Fe(\mathbf{L^{2pyridimidine}})_2(NCBH_3)_2]$	2:1	47
	$[Fe(\mathbf{L^{2pyridimidine}})_2(NCBH_3)_2]$	6:1	59
	$[Fe(\mathbf{L^{4pyridimidine}})_2(NCBH_3)_2]$	2:1	49
	$[Fe(\mathbf{L^{4pyridimidine}})_2(NCBH_3)_2]$	6:1	59
	$[Fe(\mathbf{L^{2pyridimidine}})_3](BF_4)_2$	3:1	228
	$[Fe(\mathbf{L^{2pyridimidine}})_3](BF_4)_2$	6:1	254
	$[Fe(\mathbf{L^{4pyridimidine}})_3](BF_4)_2$	3:1	246
	$[Fe(\mathbf{L^{4pyridimidine}})_3](BF_4)_2$	6:1	264
acetone	$\mathbf{L^{2pyridimidine}}$	-	0.8
	$\mathbf{L^{4pyridimidine}}$	-	0.8
	$[Fe(pyridine)_2(NCBH_3)_2]$	-	13
	$[Fe(H_2O)_3](BF_4)_2$	-	251
	$[Fe(\mathbf{L^{2pyridimidine}})_2(NCBH_3)_2]$	2:1	15
	$[Fe(\mathbf{L^{2pyridimidine}})_2(NCBH_3)_2]$	6:1	19
	$[Fe(\mathbf{L^{4pyridimidine}})_2(NCBH_3)_2]$	2:1	14
	$[Fe(\mathbf{L^{4pyridimidine}})_2(NCBH_3)_2]$	6:1	17
	$[Fe(\mathbf{L^{2pyridimidine}})_3](BF_4)_2$	3:1	221
	$[Fe(\mathbf{L^{2pyridimidine}})_3](BF_4)_2$	6:1	235
	$[Fe(\mathbf{L^{4pyridimidine}})_3](BF_4)_2$	3:1	224
	$[Fe(\mathbf{L^{4pyridimidine}})_3](BF_4)_2$	6:1	252

S7. References

1. *CryAlisPRO*, Oxford Diffraction: **2011**.
2. Sheldrick, G. M. *SADABS. Empirical absorption correction program for area detector data*, University of Göttingen, Germany, **1996**.
3. *CrysAlisPro*, CrysAlisPro, Version 171.37.33; Agilent Technologies: Yarnton, Oxfordshire, **2014**.
4. Palatinus, L.; Chapuis, G., SUPERFLIP. A computer program for the solution of crystal structures by charge flipping in arbitrary dimensions. *J. Appl. Crystallogr.,* **2007,** *40*, 786-790.
5. Sheldrick, G. M., A short history of *SHELX*. *Acta Crystallogr., Sect. A: Found. Crystallogr.,* **2008,** *A64*, 112-122.
6. Taratula, O.; Hill, P. A.; Khan, N. S.; Carroll, P. J.; Dmochowski, I. J., Crystallographic observation of 'induced fit' in a cryptophane host–guest model system. *Nature Communications,* **2010,** *1*, 148.
7. van der Sluis, P.; Spek, A. L., BYPASS: an effective method for the refinement of crystal structures containing disordered solvent regions. *Acta Crystallogr., Sect. A: Found. Crystallogr.,* **1990,** *A46*, 194-201.
8. Miller, R. G.; Brooker, S., Reversible quantitative guest sensing via spin crossover of an iron(II) triazole. *Chem. Sci.,* **2016,** *7*, 2501-2505 and front cover feature.
9. Rodríguez-Jiménez, S.; Feltham, H. L. C.; Brooker, S., Non-porous iron(II)-based sensor: crystallographic insights into a cycle of colorful guest-induced topotactic transformations. *Angew. Chem. Int. Ed.,* **2016,** *55*, 15067–15071 and back cover.
10. Rodríguez-Jiménez, S.; Yang, M.; Stewart, I.; Garden, A. L.; Brooker, S., A simple method of predicting spin state in solution. *J. Am. Chem. Soc.,* **2017,** *139*, 18392–18396.
11. Rodríguez-Jiménez, S. Spin crossover by design PhD thesis, University of Otago, New Zealand, 2017.
12. Evans, D. F., The determination of the paramagnetic susceptibility of substances in solution by nuclear magnetic resonance. *J. Chem. Soc.,* **1959**, 2003-5.
13. Piguet, C., Paramagnetic susceptibility by NMR: the 'solvent correction' removed for large paramagnetic molecules. *J. Chem. Ed.,* **1997,** *74*, 815-816.
14. Hogue, R. W.; Feltham, H. L. C.; Miller, R. G.; Brooker, S., Spin crossover in dinuclear N_4S_2 iron(II) thioether-triazole complexes: access to [HS-HS], [HS-LS] and [LS-LS] states. *Inorg. Chem.,* **2016,** *55*, 4152–4165.
15. Rodríguez-Jiménez, S.; Brooker, S., Solid Versus Solution Spin Crossover and the Importance of Fe-N≡C(X) Angle. *Inorg. Chem.,* **2017,** *56*, 13697-13708.
16. Shores, M. P.; Klug, C. M.; Fiedler, S. R., Spin-state switching in solution. In *Spin-Crossover Materials*, John Wiley & Sons Ltd: Chichester, **2013**; pp 281-301.
17. Kershaw Cook, L. J.; Kulmaczewski, R.; Mohammed, R.; Dudley, S.; Barrett, S. A.; Little, M. A.; Deeth, R. J.; Halcrow, M. A., A unified treatment of the relationship between ligand substituents and spin state in a family of iron(II) complexes. *Angew. Chem. Int. Ed.,* **2016,** *55*, 4327-4331.
18. Toftlund, H.; McGarvey, J. J., Iron(II) spin crossover systems with multidentate ligands. *Top. Curr. Chem.,* **2004,** *233*, 151-166.
19. Yatsunyk, L. A.; Walker, F. A., Structural, NMR, and EPR studies of *S* = 1/2 and *S* = 3/2 Fe(III) bis(4-cyanopyridine) complexes of dodecasubstituted porphyrins. *Inorg. Chem.,* **2004,** *43*, 757-777.
20. Slichter, C. P.; Drickamer, H. G., Pressure-induced electronic changes in compounds of iron. *J. Chem. Phys.,* **1972,** *56*, 2142-2160.
21. Kahn, O., *Molecular Magnetism*. VCH Publishers Inc.: New York, **1993**.
22. Nakano, K.; Suemura, N.; Kawata, S.; Fuyuhiro, A.; Yagi, T.; Nasu, S.; Morimoto, S.; Kaizaki, S., Magnetic behavior and Mössbauer spectra of spin-crossover pyrazolate bridged dinuclear diiron(II) complexes: X-ray structures of high-spin and low-spin $[\{Fe(NCBH_3)(py)\}_2(\mu\text{-bpypz})_2]$. *Dalton Trans.,* **2004**, 982-988.
23. Reichardt, C., *Chem. Rev.,* **1994,** *94*, 2319.
24. Ahuja, S., *Chromatography and Separation Science*. Academic Press: **2003**.
25. Schirmer, R. E., *Modern Methods of Pharmaceutical Analysis, Second Edition*. Taylor & Francis: **1990**.
26. Marcus, Y., The properties of organic liquids that are relevant to their use as solvating solvents. *Chem. Soc. Rev.,* **1993,** *22*, 409-416.

27. Swain, C. G.; Swain, M. S.; Powell, A. L.; Alunni, S., Solvent effects on chemical reactivity. Evaluation of anion- and cation-solvation components. *J. Am. Chem. Soc.,* **1983,** *105*, 502-513.

28. Barton, A. F. M., Solubility parameters. *Chem. Rev.,* **1975,** *75*, 731-753.

29. Spingler, B.; Schnidrig, S.; Todorova, T.; Wild, F., Some thoughts about the single crystal growth of small molecules. *CrystEngComm,* **2012,** *14*, 751-757.

30. Snyder, L. R., Classification of the solvent properties of common liquids. *J. Chromatogr. A,* **1974,** *92*, 223-230.

31. Kamlet, M. J.; Abboud, J. L. M.; Abraham, M. H.; Taft, R. W., Linear solvation energy relationships. 23. A comprehensive collection of the solvatochromic parameters, *p**, *a*, and *b*, and some methods for simplifying the generalized solvatochromic equation. *J. Org. Chem.,* **1983,** *48*, 2877-2887.

32. Catalán, J.; Díaz, C.; López, V.; Pérez, P.; De Paz, J.-L. G.; Rodríguez, J. G., A Generalized Solvent Basicity Scale: The Solvatochromism of 5-Nitroindoline and Its Homomorph 1-Methyl-5-nitroindoline. *Liebigs Ann. Chem.,* **1996,** *1996*, 1785-1794.

33. Gutmann, V., *The Donor-Acceptor Approach to Molecular Interaction*. Plenum Press: New York, **1978**.

34. Gutmann, V.; Wychera, E., Coordination reactions in non aqueous solutions - The role of the donor strength. *Inorg. Nucl. Chem. Lett.,* **1966,** *2*, 257-260.

35. Mayer, U.; Gutmann, V.; Gerger, W., The acceptor number — A quantitative empirical parameter for the electrophilic properties of solvents. *Monatsh. Chem.,* **1975,** *106*, 1235-1257.

36. Geary, W. J., The Use of Conductivity Measurements in Organic Solvents for the Characterisation of Coordination Compounds. *Coord. Chem. Rev.,* **1971,** *7*, 81-122.